Atmospheric Environment 198 (2019) 496–509

Contents lists available at ScienceDirect

Atmospheric Environment

journal homepage: www.elsevier.com/locate/atmosenv

# Quantifying stratosphere-troposphere transport of ozone using balloon-borne ozonesondes, radar windprofilers and trajectory models

D.W. Tarasick[a,*], T.K. Carey-Smith[b], W.K. Hocking[c], O. Moeini[a], H. He[a], J. Liu[d,e], M.K. Osman[f], A.M. Thompson[g], B.J. Johnson[h], S.J. Oltmans[h], J.T. Merrill[i]

[a] Air Quality Research Division, Environment and Climate Change Canada, Downsview, ON, M3H 5T4, Canada
[b] National Institute of Water and Atmospheric Research Ltd., Private Bag, 14901, Kilbirnie, Wellington, New Zealand
[c] Department of Physics and Astronomy, University of Western Ontario, London, ON, N6A 3K7, Canada
[d] Department of Geography and Planning, University of Toronto, Canada
[e] School of Atmospheric Sciences, Nanjing University, Nanjing, China
[f] Cooperative Institute for Mesoscale Meteorological Studies, The University of Oklahoma, and NOAA/National Severe Storms Laboratory, Norman, OK, USA
[g] NASA Goddard Space Flight Center, Greenbelt, MD, USA
[h] Global Monitoring Division, Earth System Research Laboratory, National Oceanic and Atmospheric Administration, Boulder, CO, USA
[i] Graduate School of Oceanography, University of Rhode Island, RI, USA

ARTICLE INFO

*Keywords:*
Ozone
Ozonesondes
Stratospheric intrusions
Stratospheretroposphere
Transport
Radar windprofilers

ABSTRACT

In a series of 10-day campaigns in Ontario and Quebec, Canada, between 2005 and 2007, ozonesondes were launched twice daily in conjunction with continuous high-resolution wind-profiling radar measurements. Windprofilers can measure rapid changes in the height of the tropopause, and in some cases follow stratospheric intrusions. Observed stratospheric intrusions were studied with the aid of a Lagrangian particle dispersion model and the Canadian operational weather forecast system. Definite stratosphere-troposphere transport (STT) events occurred approximately every 2–3 days during the spring and summer campaigns, whereas during autumn and winter, the frequency was reduced to every 4–5 days. Although most events reached the lower troposphere, only three events appear to have significantly contributed to ozone amounts in the surface boundary layer. Detailed calculations find that STT, while highly variable, is responsible for an average, over the seven campaigns, of 3.1% of boundary layer ozone (1.2 ppb), but 13% (5.4 ppb) in the lower troposphere and 34% (22 ppb) in the middle and upper troposphere, where these layers are defined as 0–1 km, 1–3 km, and 3–8 km respectively. Estimates based on counting laminae in ozonesonde profiles, with judicious choices of ozone and relative humidity thresholds, compare moderately well, on average, with these values. The lamina detection algorithm is then applied to a large dataset from four summer ozonesonde campaigns at 18 North American sites between 2006 and 2011. The results show some site-to-site and year-to-year variability, but stratospheric ozone contributions average 4.6% (boundary layer), 15% (lower troposphere) and 26% (middle/upper troposphere). Calculations were also performed based on the TOST global 3D trajectory-mapped ozone data product. Maps of STT in the same three layers of the troposphere suggest that the STT ozone flux is greater over the North American continent than Europe, and much greater in winter and spring than in summer or fall. When averaged over all seasons, magnitudes over North America show similar ratios between levels to the previous calculations, but are overall 3–4 times smaller. This may be because of limitations (trajectory length and vertical resolution) to the current TOST-based calculation.

## 1. Introduction

Tropospheric ozone, particularly at ground level, is considered an air pollutant when it exceeds natural levels: it is responsible for significant damage to forests and crops (Avnery et al., 2011; McGrath et al., 2015), and is a principal factor in air quality as it has adverse effects on human respiratory health (e.g., Jerrett et al., 2009; Silva et al., 2013; Bell et al., 2014; Szyszkowicz and Rowe, 2016). Ozone affects the oxidizing capacity of the lower atmosphere (it is a primary precursor to the formation of OH radicals) and thereby influences the lifetime of methane, more complex hydrocarbons, and most other reactive trace gases in the lower atmosphere (Calvert et al., 2015). Ozone

* Corresponding author.
*E-mail address:* david.tarasick@canada.ca (D.W. Tarasick).

https://doi.org/10.1016/j.atmosenv.2018.10.040
Received 1 August 2018; Received in revised form 19 October 2018; Accepted 22 October 2018
Available online 24 October 2018

is also a short-lived climate pollutant (SLCP). It is the third most important greenhouse gas, after $CO_2$ and methane, with a forcing that is strongly altitude-dependent (IPCC, 2013), and largest in the upper troposphere and lower stratosphere (IPCC, 2001).

The stratosphere is a large reservoir of ozone, but due to its high stability there is relatively little exchange of mass across its lower boundary, the tropopause. Attempts to estimate the contribution of cross-tropopause transport to the tropospheric ozone budget have been made since the 1960s (e.g. Junge, 1962; Fabian and Pruchniewicz, 1977). Stratospheric ozone enters the troposphere primarily through a variety of irreversible eddy exchange phenomena that are small-scale manifestations of the global, wave-driven (Brewer-Dobson) circulation, which transports ozone and other chemical species from equator to pole (Holton et al., 1995). For this reason the global flux is moderately well-estimated by models; however stratosphere-troposphere transport (STT) events are sporadic, and so the regional flux of ozone varies (Stohl et al., 2003a; b) and is not well characterized. Observational studies in North America and Europe, where STT is expected to be strongest (Wernli and Bourqui, 2002; Holton et al., 1995), have shown that variations in ozone mixing ratio in both the upper and lower troposphere are well correlated with lower stratospheric values (Tarasick et al., 2005; Ordonnez et al., 2007), but efforts to quantify the contribution of STT to the tropospheric ozone budget from observations have yielded somewhat variable results (Trickl et al., 2010). Elbern et al. (1997) found 3–4% of surface ozone at mountain sites in Europe to be attributable to STT, and Zanis et al. (2003) found contributions of 5–6.5%, while Stohl et al. (2000) estimated 7–15% from observations and 15–25% from FLEXPART modeling, for a similar set of locations. Dibb et al. (1994) found a (springtime) maximum of 10–15% of surface ozone from STT at a site in the Canadian Arctic, and Cristofanelli et al. (2010) also found a strong seasonality and an annual average of 14% at a site in the Himalayas at 5079 m. Colette and Ancellet (2005), using data from 11 ozonesonde stations in Europe, assigned about 40% of free tropospheric ozone (as a fraction of the total tropospheric column) to the stratospheric source. This is somewhat greater than the 16–34% estimated by Thompson et al. (2007a,b) at the 12 ozonesonde sites in North America during the INTEX Ozonesonde Network Study 2004 (IONS-04). These studies used different observational criteria to classify layers in ozone soundings, however. Cooper et al. (2006), using the potential vorticity-based FLEXPART retroplume technique, estimated that between 13 and 27% of ozone in the upper troposphere at IONS-04 sites was of recent stratospheric origin. This is much less than the 80% or greater fraction found by Bachmeier et al. (1994) or Dibb et al. (2003), in separate aircraft campaigns over northern North America.

Stratospheric intrusions are occasionally observed to reach the ground (Chung and Dann, 1985; Wakamatsu et al., 1989; Davies and Schuepbach, 1994; Eisele et al., 1999; Cooper and Moody, 2000; Cooper et al., 2005; Langford et al., 2012), but much more frequently, intrusion events reach the upper or middle troposphere, where they appear to dissipate and contribute to the general free tropospheric ozone burden (e.g. Colette and Ancellet, 2005; Hocking et al., 2007). This implies that changes in STT could affect the radiative forcing of ozone, which depends on the vertical distribution of ozone in the troposphere, and is largest near the tropopause. Climate change is expected to increase planetary wave activity and so cause an accelerated Brewer-Dobson circulation (e.g. Butchart et al., 2006, 2014). The projected acceleration, along with stratospheric ozone recovery, will lead to increased transport of ozone from the stratosphere into the troposphere (Randel and Thompson, 2011; Sioris et al., 2014; Banerjee et al., 2016). This is expected to increase tropospheric ozone concentrations (Neu et al., 2014; Hess and Zbinden, 2013; Fusco and Logan, 2003).

Modeling and ozonesonde studies (e.g. Bourqui and Trépanier, 2010; Cooper et al., 2011; He et al., 2011; Dempsey, 2014), as well as reanalyses (Knowland et al., 2017) link STT and ground-level ozone, but the exchange of ozone between the free troposphere and the boundary layer is not well understood. Recent studies suggest that the influence of stratospheric intrusions on near-surface background ozone is of greater importance than previously anticipated (Bourqui and Trépanier, 2010; Lin et al., 2012; Lefohn et al., 2014), and that their overall effect on boundary layer ozone may be underestimated (Zanis et al., 2014; Akritidis et al., 2016; Langford et al., 2018).

The results of several 10-day campaigns in Ontario and Quebec, Canada between 2005 and 2007 are described here. Ozonesondes were launched twice daily in conjunction with continuous high-resolution wind-profiling radar measurements. Intrusion events identified in ozone soundings were confirmed by model calculations, using the Lagrangian particle dispersion model FLEXPART (Stohl et al., 2005) with (hourly) meteorological input from version 3.2.0 of GEM, the Canadian operational forecast model, with 58 vertical levels on the standard regional domain covering North America. The observed frequency of STT events is discussed and their impact on tropospheric ozone levels is quantified using GEM-FLEXPART, and compared to additional estimates from extensive summertime ozonesonde campaigns in North America, and using data from the global network of ozone soundings archived in the World Ozone and UV Data Centre (WOUDC), coupled with calculations using the Hybrid Single-Particle Lagrangian Integrated Trajectory (HYSPLIT) model (Draxler and Hess, 1998) and archived meteorological fields from National Centers for Environmental Prediction (NCEP).

## 2. Observations

A series of ozonesonde campaigns was conducted between 2005 and 2007, in conjunction with continuous high-resolution wind-profiling radar observations, to investigate STT.

The balloon-borne instruments used were GPS-equipped EN-SCI 2Z ECC ozonesondes and Vaisala RS80 radiosondes, providing vertical profiles of ozone concentration, temperature, humidity, wind speed and wind direction. Electrochemical concentration cell (ECC) ozonesondes have a precision of 3–5% and an absolute accuracy of about 10% in the troposphere (Smit et al., 2007; Tarasick et al., 2018). The ozone sensor $e^{-1}$ response time of about 25 s gives the sonde a vertical resolution of about 100–125 m for a typical balloon ascent rate of 4–5 m/s in the troposphere. They were released approximately twice daily near the radar sites located at Montreal (45.4 N, 73.9 W), and Walsingham (42.6 N, 80.6 W) and Harrow (42.0 N, 82.9 W) in Ontario. At Walsingham and Harrow, the launches took place at the radar site. In the Montreal case, the launches were performed from the headquarters of the Canadian Space Agency Head Office in St. Hubert, Quebec, while the radar was located at the MacDonald campus of McGill University, about 45 km distant. The windprofiler radars were WindTtracker radars, a commercially available instrument that provides real-time wind information as a function of height and time, and also measurements of backscattered power, turbulence strengths, tropopause heights, and turbulence anisotropy (Hocking, 1997). The radars are part of the Ontario-Quebec VHF windprofiler radar network (O-QNet).

Ozonesonde campaigns were also conducted in June, July and August of 2006 and 2008 from sites across North America in the INTEX Ozonesonde Network Study (IONS) campaigns (Thompson et al., 2007a,b, 2010; Tarasick et al., 2010), and in the 2010 and 2011 BORTAS (Quantifying the impact of BOReal forest fires on Tropospheric oxidants using Aircraft and Satellites) campaigns (Palmer et al., 2013). A total of 1110 profiles from sites north of 40° latitude have been used here (Fig. 1 and Table 1). Two types of ECC ozonesondes, the 2Z model manufactured by EnSci Corp. and the 6A model manufactured by Science Pump, with minor differences in construction and preparation, were used at different sites. The maximum likely variation in tropospheric response resulting from these differences is of the order of 2–3% (Smit et al., 2007), and for these purposes is a negligible source of error.

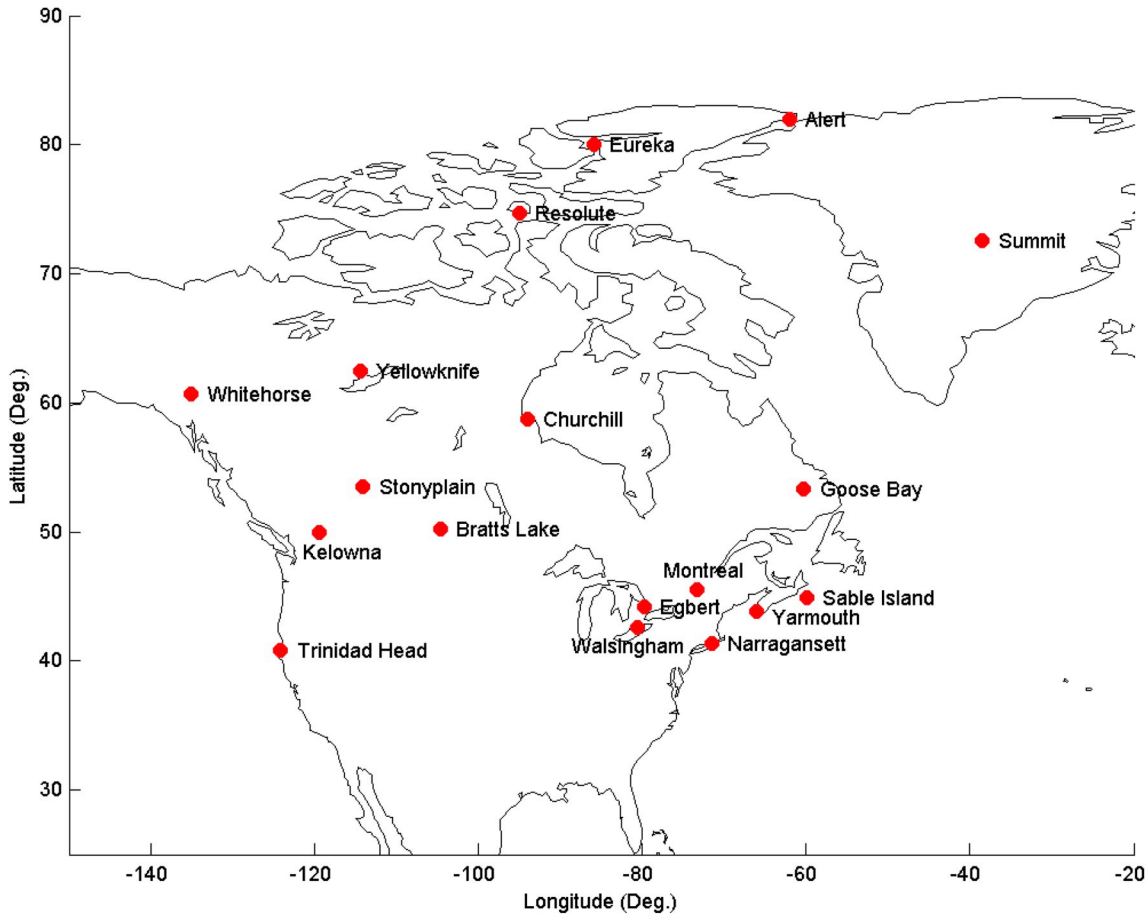


**Fig. 1.** Location of stations participating in the IONS and BORTAS campaigns.

## 3. Models

The vertical ozone distribution in each of the radar-ozonesonde campaigns was compared with model results from the Lagrangian particle dispersion model FLEXPART (Stohl et al., 2005), run in forward mode. Input to FLEXPART was provided by version 3.2.0 of GEM, the Canadian forecast model. The standard regional domain covering North America with 58 vertical levels to 10 hPa was used. The model was run forward for 12 h starting from analysis fields at 12 hourly intervals, producing hourly output fields. The native output from GEM was interpolated onto a 0.5 × 0.5° resolution latitude-longitude grid and then converted into the GRIB format necessary for input to FLEXPART. In

**Table 1**
Number of profiles per month at each site in the IONS and BORTAS campaigns.

| | 2006 | | | 2008 | | | 2010 | | | 2011 | | | Total |
|---|---|---|---|---|---|---|---|---|---|---|---|---|---|
| Site Name | Jun | Jul | Aug | Jun | Jul | Aug | Jun | Jul | Aug | Jun | Jul | Aug | |
| Alert | 4 | 3 | 5 | 4 | 4 | 5 | 4 | 2 | 2 | 3 | 3 | 4 | 43 |
| Eureka | 3 | 4 | 5 | 4 | 4 | 5 | 5 | 3 | 3 | 5 | 4 | 5 | 50 |
| Resolute | 3 | 1 | 0 | 3 | 5 | 3 | 4 | 2 | 3 | 2 | 2 | 1 | 29 |
| Summit | 5 | 4 | 2 | 15 | 26 | 4 | 3 | 2 | 4 | 5 | 4 | 5 | 79 |
| Whitehorse | 0 | 0 | 0 | 7 | 11 | 0 | 0 | 0 | 0 | 0 | 0 | 0 | 18 |
| Yellowknife | 0 | 0 | 0 | 4 | 11 | 0 | 0 | 0 | 0 | 0 | 0 | 0 | 15 |
| Churchill | 4 | 4 | 4 | 8 | 8 | 1 | 2 | 4 | 3 | 5 | 1 | 1 | 45 |
| Trinidad | 5 | 4 | 30 | 10 | 15 | 4 | 18 | 3 | 4 | 4 | 4 | 4 | 105 |
| Kelowna | 5 | 2 | 27 | 8 | 13 | 4 | 18 | 2 | 3 | 2 | 3 | 5 | 92 |
| Stonyplain | 4 | 1 | 4 | 8 | 14 | 3 | 5 | 4 | 3 | 5 | 4 | 5 | 60 |
| Bratt's Lake | 4 | 2 | 29 | 6 | 11 | 4 | 4 | 17 | 4 | 4 | 21 | 5 | 111 |
| Walsingham | 0 | 0 | 22 | 0 | 0 | 0 | 0 | 12 | 0 | 0 | 0 | 0 | 34 |
| Egbert | 3 | 4 | 15 | 1 | 12 | 3 | 4 | 20 | 5 | 5 | 17 | 4 | 93 |
| CSA-Montreal | 0 | 0 | 0 | 0 | 0 | 0 | 0 | 14 | 0 | 0 | 0 | 0 | 14 |
| Narragansett | 4 | 4 | 24 | 4 | 3 | 5 | 2 | 2 | 2 | 0 | 0 | 0 | 50 |
| Yarmouth | 3 | 3 | 11 | 8 | 14 | 1 | 5 | 20 | 8 | 5 | 20 | 7 | 105 |
| Goose Bay | 3 | 2 | 5 | 4 | 11 | 0 | 4 | 18 | 8 | 4 | 22 | 7 | 88 |
| Sable Island | 0 | 0 | 28 | 4 | 11 | 0 | 0 | 16 | 0 | 0 | 19 | 1 | 79 |
| **Total** | 50 | 38 | 211 | 98 | 173 | 42 | 78 | 141 | 52 | 49 | 124 | 54 | 1110 |

forward mode, FLEXPART uses a domain filling procedure where a large number of particles (~600,000 in each case discussed below) are released within the model domain at the beginning of a model run. During model initialization, particles which are in the stratosphere (those having a potential vorticity greater than 2 PVU, where 1 PVU = $10^{-6}m^2kg^{-1}s^{-1}$) are tagged with an ozone concentration. This is calculated using the average value of measured ozone to modeled PV over each campaign period. These particles are then advected using model wind fields. New particles are created and initialized in the same way on in-flow boundaries.

FLEXPART does not include any chemistry and ozone is assumed to have an infinite lifetime once in the troposphere. This assumption is reasonable as none of the simulations went beyond 10 days, while the lifetime of ozone in the troposphere is typically 20–30 days (Stevenson et al., 2013). In addition, because of the limited domain size, any particular particle is unlikely to stay within the domain for that length of time. The limited domain size also means that particles that crossed from the stratosphere before entering the domain will have zero ozone concentration. In other words, only intrusions that occur within the domain are simulated.

The Trajectory-mapped Ozonesonde dataset for the Stratosphere and Troposphere (TOST) is a global three-dimensional ozone data product that is derived from ozone soundings archived in the World Ozone and UV Date Centre (WOUDC). It uses the Hybrid Single-Particle Lagrangian Integrated Trajectory (HYSPLIT) model (Draxler and Hess, 1998) and meteorological fields from National Centers for Environmental Prediction (NCEP) reanalyses to fill the gaps between ozonesonde stations, by extending each ozone record along its trajectory path forward and backward for 4 days. Over this 4-day period ozone production and loss along the path is assumed to be negligible. Ozone values along these trajectory paths are binned into a 3-dimensional grid of 5° × 5° x 1 km (latitude, longitude, and altitude), from ground level up to 26 km. Over 67,000 ozonesonde profiles at 116 stations from 1965 to 2012 are used. TOST has been evaluated using individual ozonesondes, excluded from the mapping, by backward and forward trajectory comparisons, and by comparisons with aircraft profiles and surface monitoring data (Tarasick et al., 2010; Liu et al., 2013a,b). Differences are typically about 10% or less, but there are larger biases in the UTLS, the boundary layer, and in areas where ozonesonde measurements are sparse.

For use in models that have a dynamically-determined tropopause, TOST is produced in troposphere-only, stratosphere-only, and combined versions. Statistical parameters such as number of trajectories contributing to each grid cell are also calculated. These ancillary products offer the possibility of estimating the stratospheric contribution to ozone at different levels in the troposphere. Using the forward trajectories for the stratosphere-only dataset, which employs only trajectories that start above the (thermal) tropopause, it is possible to estimate STT by comparing to the full stratosphere-troposphere dataset. As trajectories are limited to 4 days in the version currently available, they are less subject to errors, which grow significantly with trajectory length (Stohl, 1998), but they represent fast STT, and may miss longer-term STT contributions to tropospheric ozone.

## 4. Radar and ozonesonde results

Previous work (Hocking et al., 2007) demonstrated, using wind-profiling radar and multiple ozone soundings, that intrusions of stratospheric ozone into the troposphere can be predicted by rapid changes in tropopause height, and that intrusion events are quite frequent at midlatitudes in Canada. Fig. 2 (left) shows vertical profiles of ozone mixing ratio for the May 2005 campaign at Montreal, Quebec. From 29 April to 10 May 2005, ozonesondes were launched every 12 h at 00 UT and 12 UT. The radar-derived tropopause height is shown as a solid white line. This is calculated by first averaging the radar power over 2 h to provide a vertical profile with 500 m height resolution. The gradient at each point in this profile is then found by fitting a straight line over a height of 1500 m. The four points above 5.75 km having the largest gradients are extracted. The point with the largest gradient is taken to be the tropopause point, unless one or more of the other three are contiguous to it, in which case an average is taken of the contiguous points, weighted by the magnitude of each associated gradient.

A number of major changes in tropopause height are apparent, as well as layers of high ozone, which generally appear to descend from left to right; i.e. with time. However, the continuity of these layers is not always clear, as the sampling is one-dimensional in space. The right-hand plot shows a plot of results from a GEM-FLEXPART simulation, showing the 40-ppb isopleth of ozone transported from the stratosphere, at 06 UT on 5 May 2005. At this time the deep tongue of the intrusion is to the southwest of the Montreal site, and so would be missed by a vertical sounding.

At several points on the left-hand plot the tropopause shows a rapid increase in apparent height (indicated by dashed vertical lines). In most cases these represent real changes in the local tropopause height, as the

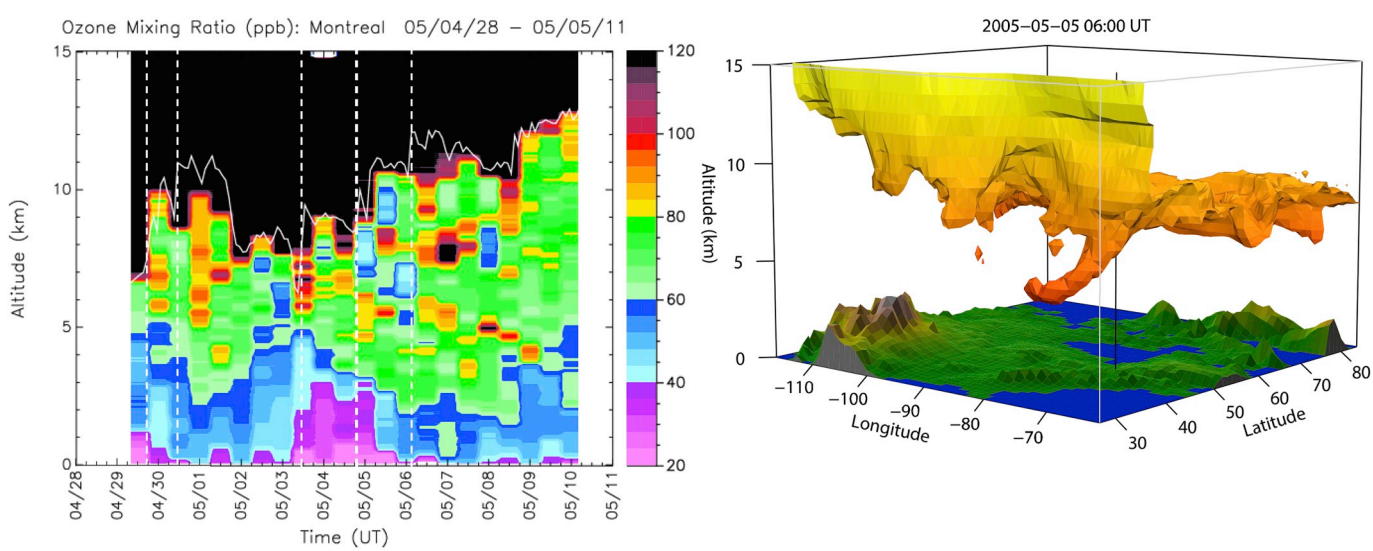


**Fig. 2.** Left: Vertical profiles of ozone mixing ratio for the May 2005 campaign at Montreal, Quebec. The solid white line shows the tropopause height derived from the radar data. The dashed white lines indicate times when the tropopause height appears to increase rapidly. Right: FLEXPART output showing the 40-ppb isopleth of ozone transported from the stratosphere, at 06 UT on 5 May 2005. The vertical black line shows the location of the McGill University wind-profiling radar.

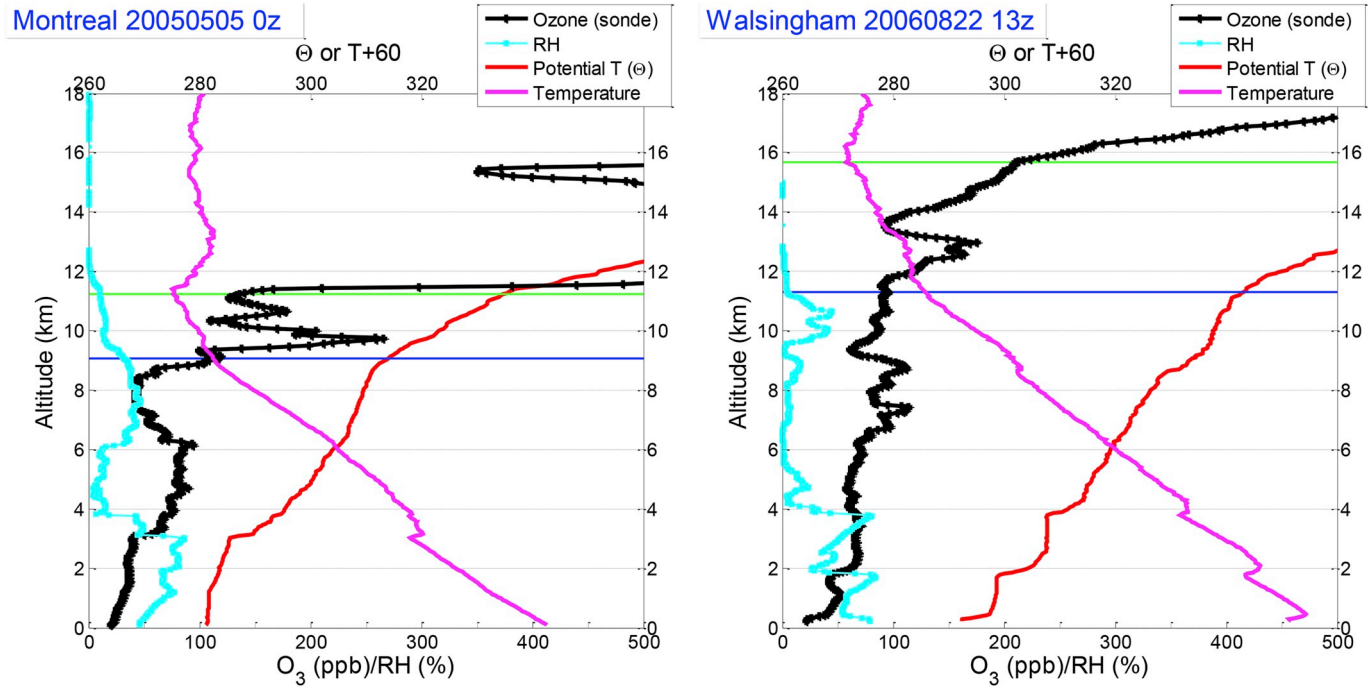


**Fig. 3.** Ozone and water-vapour pressure profiles taken at Montreal and Walsingham, Ontario. The green line indicates the WMO (temperature lapse rate) tropopause; the blue line the radar tropopause. (For interpretation of the references to colour in this figure legend, the reader is referred to the Web version of this article.)

passage of upper level cyclones temporarily force the polar jet stream north of the observing location. Such disturbances are known to be associated with STT (Johnson and Viezee, 1981; Danielsen, 1968).

While the tropopause height determined by the radar is typically identical to that using the standard thermal lapse rate definition (WMO, 1966), this is not always the case. Hooper and Arvelius (2000), comparing several measures of tropopause height, found that while the radar tropopause showed good agreement with the thermal tropopause, it correlated more strongly with the ozone tropopause. The backscattered power for a VHF radar is approximately proportional to $M^2/r^2$, where $r$ is the range from the radar and $M$ is the vertical gradient of the potential refractive index

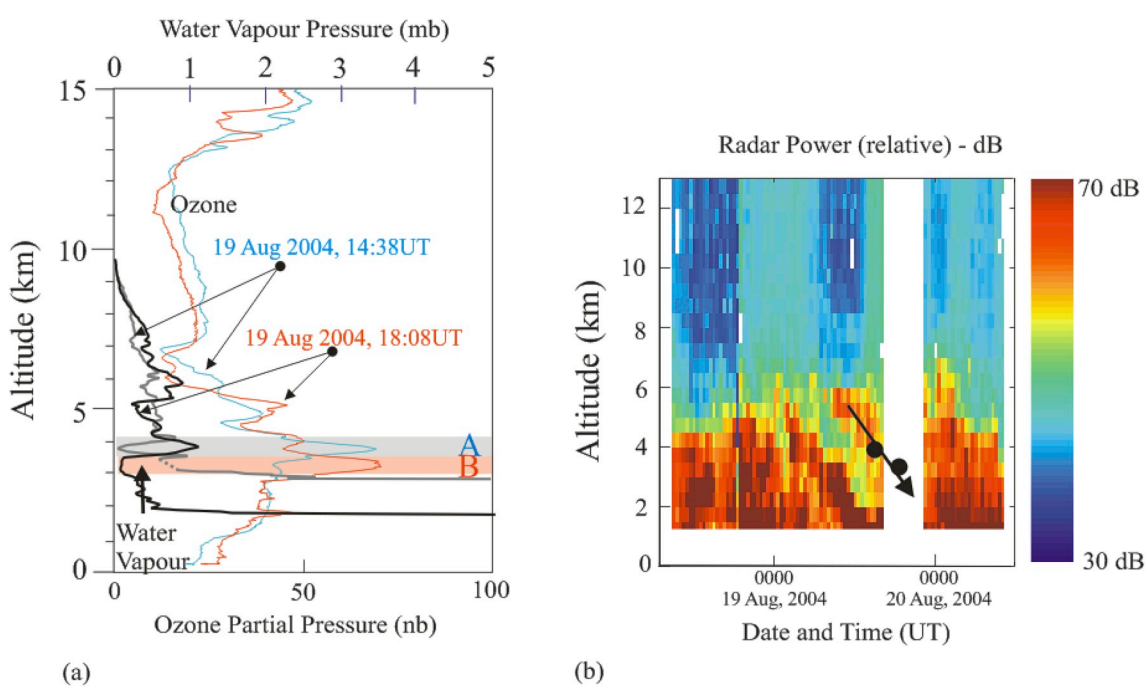


**Fig. 4.** (a) Successive ozone and water-vapour pressure profiles taken only four hours apart on 19 August 2004. Movement can be seen, as peak A moves to peak B. Graph (b) shows radar backscattered power as a function of time and height from 18 to 20 August 2004. The peaks A and B have high ozone but low water vapour, and steep gradients in water vapour at their edges. These water vapour gradients produce enhanced radio backscatter, and the radar signal enhancement shown in 4b by the downward sloping arrow in fact tracks the ozone maximum. The two black dots in that figure show the height of the peaks in ozone density for events A and B (although unfortunately the radar was not operational for case B).

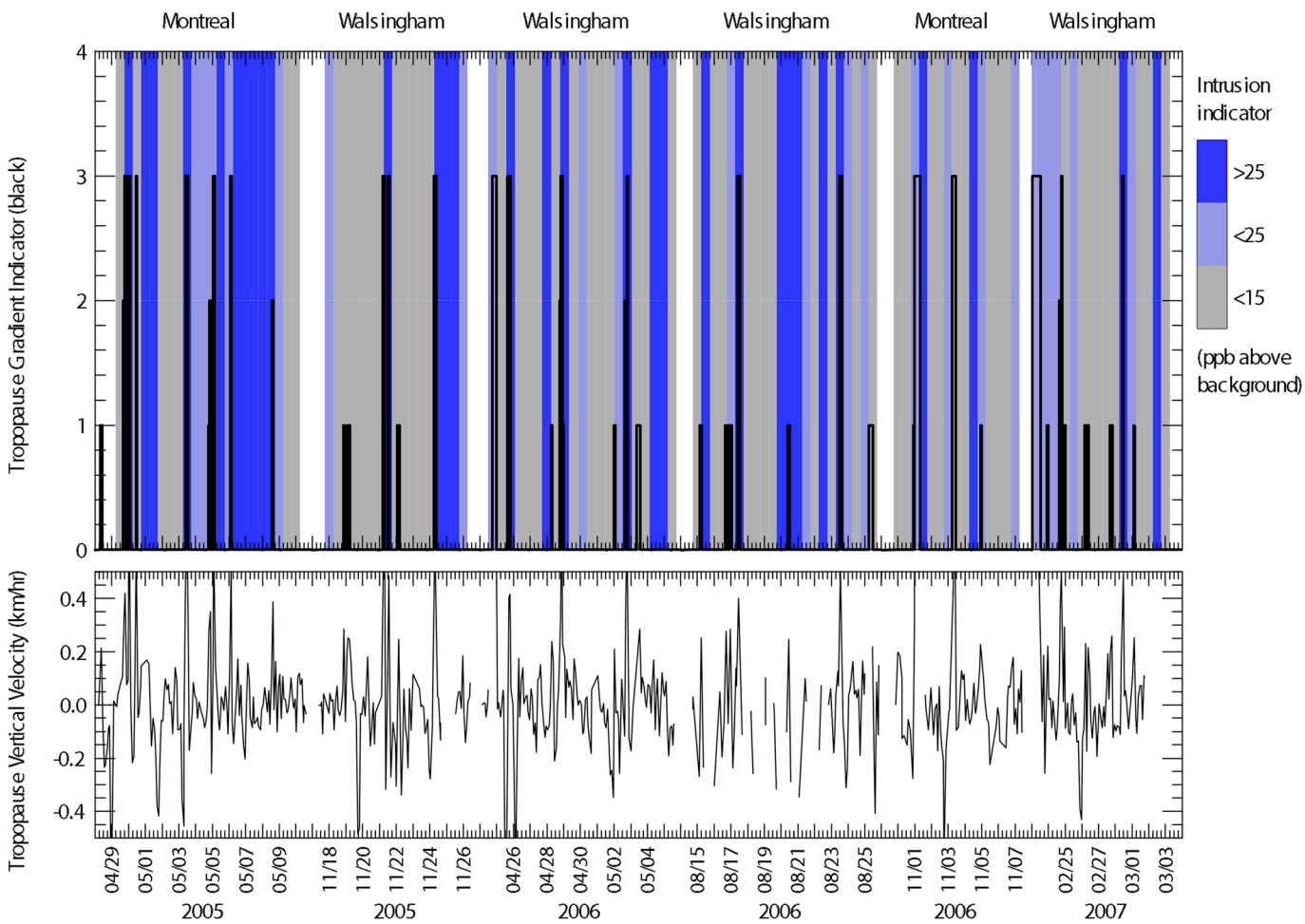


**Fig. 5.** Comparison between the rate of change of the radar-derived tropopause height and observational evidence of STE. Note the discontinuities in the time axis. Bottom panel: change in radar-derived tropopause height in units of km $hr^{-1}$. Increases in tropopause height where the apparent vertical velocity of the tropopause exceeds 0.4 km $h^{-1}$ are depicted in the upper panel by the black bars having a tropopause gradient indictor of value 3. Tropopause gradient indictors of 2 and 1 correspond to vertical velocities greater than 0.3 and 0.2 km $h^{-1}$, respectively. Smaller rates of change are not shown. The shading in the upper panel denotes when a possible stratospheric intrusion of ozone was observed in the ozonesonde profiles. This intrusion indicator was calculated by estimating the difference in ozone mixing ratio between the peak of the possible intrusion and the mean of the surrounding region (above, below, before and after the enhanced region).

$$M = 7.76 \times 10^{-5}\left(\frac{p}{T}\right)\left(\frac{\partial \ln \theta}{\partial z}\right)\left[1 + \frac{15500q}{T}\left[1 - \frac{\frac{\partial \ln q}{\partial z}}{2\frac{\partial \ln \theta}{\partial z}}\right]\right] \quad (1)$$

where $\theta$ (K) is potential temperature, $T$ is temperature, $p$ (hPa) is pressure, $z$ (m) is altitude, and $q$ is specific humidity (Vanzandt et al., 1978). The term in square brackets is generally small, as $q$ is small above the lower troposphere, and the radar usually detects a maximum in backscatter at the abrupt change in the gradient of potential temperature at the tropopause. However, in some cases a change in $\partial \ln \theta / \partial z$ below the tropopause, often coincident with a sharp negative gradient of water vapour, can produce a larger maximum. In these cases soundings show dynamically disturbed profiles of temperature, ozone and water vapour, and it appears that the radar is in fact detecting the sharp increase in potential temperature and decrease in water vapour associated with an intrusion of stratospheric air. In the cases shown in Fig. 3, the sharp negative gradients of water vapour actually contribute significantly to the backscatter, as $\partial \ln q$ is much larger than $\partial \ln \theta$, and the factor in square brackets is about 1.2 even though $q$ is very small.

Cases like those in Fig. 3, where the radar-derived tropopause height differs from the WMO (temperature lapse rate) tropopause are uncommon, and appear to be due to the radar detecting an intrusion of stratospheric air. This is especially clear in the first example (Montreal). In every observed case the radar soon afterward reverts to detecting the thermal tropopause. This produces an apparent rapid change in the radar-derived tropopause height.

In the lower troposphere, where $q$ is larger, gradients of humidity can dominate the radar signal. Fig. 4 shows successive ozone and humidity profiles and simultaneous observations with the radar near London, Ontario. It is apparent that the radar can track the descent of the dry layer of high ozone.

For these reasons radar appears to be a particularly good intrusion detector, and rapid changes in radar-derived tropopause height, whether apparent (Fig. 3) or real (Fig. 2), are a good indicator of STT. Fig. 5 follows Fig. 4 of Hocking et al. (2007), while extending the data set with two more recent campaigns. The bottom panel shows the change in radar-derived tropopause height in units of km $hr^{-1}$. Increases in tropopause height where the apparent vertical velocity of the tropopause exceeds 0.4 km $h^{-1}$ are considered abrupt. Such events are depicted in the upper panel by the black bars having a tropopause gradient indictor of value 3. Tropopause gradient indictors of 2 and 1 correspond to vertical velocities greater than 0.3 and 0.2 km $h^{-1}$, respectively. Vertical velocities less than 0.2 km $h^{-1}$ are not shown in the upper panel. The shading in the upper panel denotes when a possible stratospheric intrusion of ozone was observed in the tropospheric region of the ozonesonde profiles. This intrusion indicator was calculated by estimating the difference in ozone mixing ratio between the peak of the possible intrusion and the mean of the surrounding region (above,

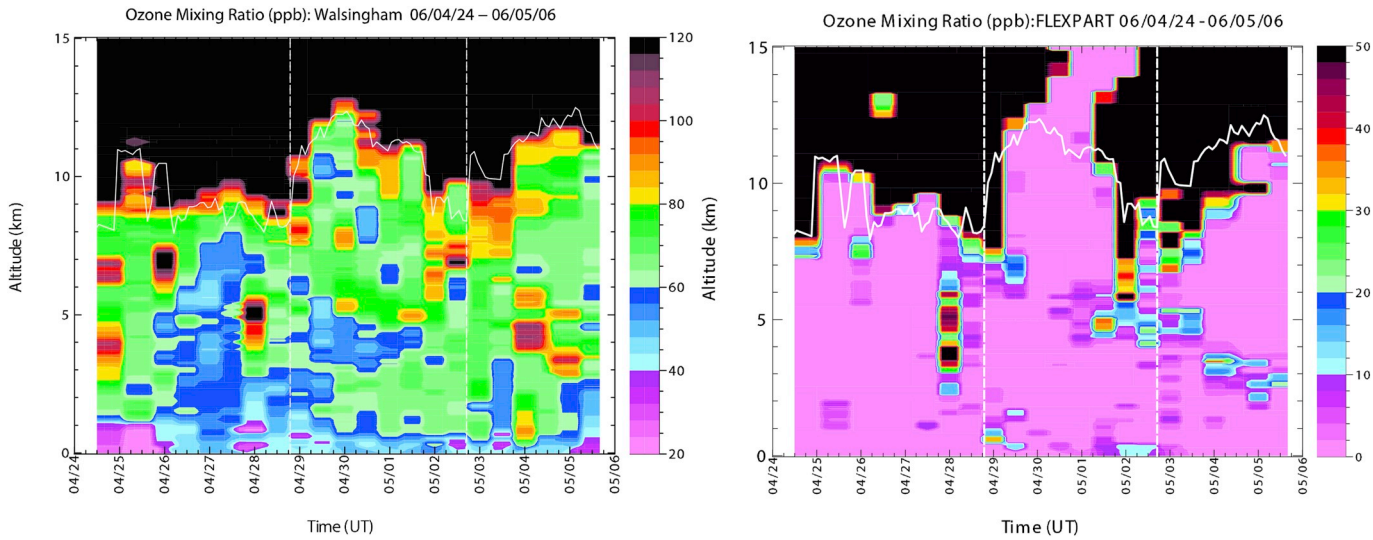


**Fig. 6.** Left: Vertical profiles of ozone mixing ratio for the April 2006 campaign at Walsingham, Ontario. The solid line shows the tropopause height derived from the radar data. The dashed lines indicate times when the tropopause height appears to increase rapidly. Right: A similar plot of ozone mixing ratio values from a GEM-FLEXPART simulation. The values were extracted from the FLEXPART output grid at locations along the sonde flight paths. Note the change in colour scale. Much of the lower part of the figure is featureless (with zero ozone) as the FLEXPART simulation does not include background tropospheric ozone. (For interpretation of the references to colour in this figure legend, the reader is referred to the Web version of this article.)

below, before and after the enhanced region). From this diagram it is clear that at or soon after each peak in the tropopause vertical velocity (level 3 tropopause gradient), either a weak or strong intrusion event takes place. Also, almost all strong intrusions that were observed follow a level 2 or 3 tropopause height increase. Of the five to six exceptions to this observation, one was when the radar was not operational (early March 2007) and three when the radar could not resolve the height of the tropopause because it was dynamically perturbed (e.g. mid-August 2006). Some notable exceptions occur in spring and summer (e.g. May 4, 2006); these may be because the polar jet is further north and so distant from the radar location. However, they are remarkably few.

There appears to be some seasonal difference in these campaigns. Although intrusion events occur in all of them, the three campaigns in spring and summer show more frequent intrusion events, occurring every 2–3 days, while for the two campaigns in late fall and one in late winter, intrusions are less frequent, typically occurring every 4–5 days.

## 5. Estimates of ozone transport into the troposphere

### 5.1. Radar-ozonesonde campaigns

Fig. 6 (left) shows vertical profiles of ozone mixing ratio for a campaign at Walsingham, Ontario from 24 April to 5 May 2006. Layers of high ozone, which generally appear to descend from left to right on the time axis, are also apparent. The right-hand plot shows values of ozone mixing ratio extracted from the three-dimensional FLEXPART

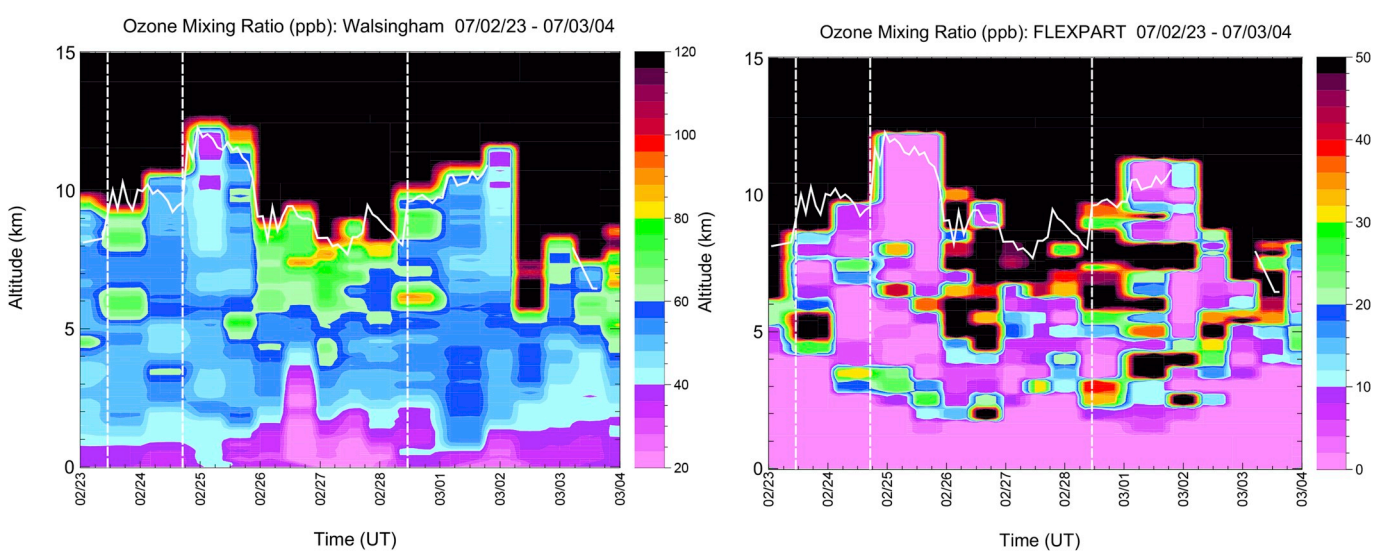


**Fig. 7.** Similar to Fig. 6, a comparison of vertical profiles of ozone mixing ratio for the February 2007 Walsingham campaign with a similar plot of ozone mixing ratio values from a GEM-FLEXPART simulation. Values in the right-hand plot were extracted from the FLEXPART output grid at locations along the sonde flight paths. Note the change in colour scale. The FLEXPART simulation includes only ozone that originates in the stratosphere. (For interpretation of the references to colour in this figure legend, the reader is referred to the Web version of this article.)

**Table 2**
Stratospheric contribution to ozone in three defined layers in the troposphere, as calculated by GEM-FLEXPART initialized with ozonesonde measurements in field campaigns. "Measured" is the observed mixing ratio, and "FLEXPART" is the calculated contribution from STT, both in ppb, while "Relative Contribution" gives the ratio of these in percent. Also shown for comparison are similar values for the STT contribution, as calculated by the ozone-RH correlation algorithm described in Section 5.2.

| Mixing Ratio | Measured (ppb) | FLEXPART (ppb) | Relative contribution | $O_3$-RH method |
|---|---|---|---|---|
| 2005-05 Montreal | | | | |
| *0-1 km* | 42 | 0.02 | 0.1% | 0 |
| *1-3 km* | 53 | 0.18 | 0.3% | 6.2% |
| *3-8 km* | 70 | 18 | 26% | 27% |
| 2005-11 Walsingham | | | | |
| *0-1 km* | 30 | 1.9 | 6.3% | 0 |
| *1-3 km* | 38 | 3.6 | 9.4% | 18% |
| *3-8 km* | 72 | 64 | 88% | 21% |
| 2006-04 Walsingham | | | | |
| *0-1 km* | 46 | 2.7 | 5.9% | 9.7% |
| *1-3 km* | 61 | 2.4 | 3.9% | 31% |
| *3-8 km* | 66 | 8.9 | 13% | 22% |
| 2006-08 Walsingham | | | | |
| *0-1 km* | 43 | 0.41 | 0.1% | 5.8% |
| *1-3 km* | 61 | 0.14 | 0.2% | 20% |
| *3-8 km* | 73 | 0.84 | 1.2% | 25% |
| 2006-10 Montreal | | | | |
| *0-1 km* | 24 | 0.13 | 0.5% | 8.5% |
| *1-3 km* | 41 | 21 | 52% | 18% |
| *3-8 km* | 51 | 16 | 33% | 19% |
| 2007-02 Walsingham | | | | |
| *0-1 km* | 32 | 0.13 | 0.4% | 0 |
| *1-3 km* | 44 | 5.1 | 12% | 13% |
| *3-8 km* | 59 | 29 | 49% | 19% |
| 2007-06 Harrow | | | | |
| *0-1 km* | 41 | 3.3 | 8% | 9.5% |
| *1-3 km* | 52 | 5.2 | 10% | 21% |
| *3-8 km* | 61 | 16 | 26% | 29% |

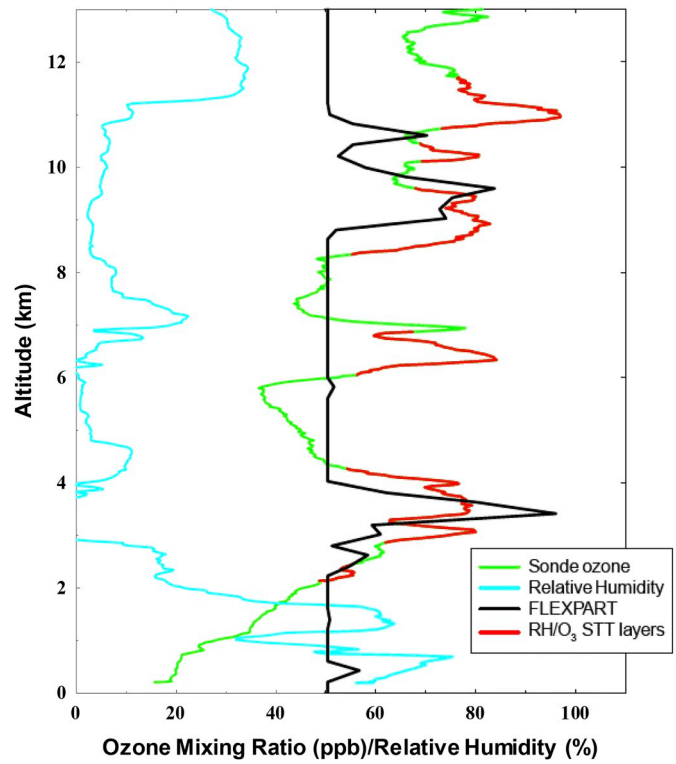


**Fig. 8.** Profiles at 12 UTC on June 29, 2007 at Harrow, Ontario. The FLEXPART profile is a six-hour average. As ozone mixing ratios from GEM-FLEXPART do not include tropospheric background ozone, the profile has been shifted by 50 ppb to more easily compare with the sonde profile. Layers in the sonde profile that are identified as STT by the RH correlation method are shown in red. Both the RH/$O_3$ correlation algorithm and the FLEXPART calculation find a number of STT layers, but the agreement is imperfect: each method finds STT layers that are not identified by the other. (For interpretation of the references to colour in this figure legend, the reader is referred to the Web version of this article.)

output grid at locations along the sonde flight paths. These values represent ozone transported from the stratosphere, as the GEM-FLEXPART simulation has no chemistry, and the model is initialized with no ozone in the troposphere. Many of the peaks observed in the sonde profiles are evident in the FLEXPART simulation, indicating a significant stratospheric contribution. The qualitative agreement between these two figures is notable, and suggests that the GEM model is reproducing the dynamics of stratospheric intrusion events and their subsequent tropospheric evolution rather well. The lack of quantitative agreement is primarily due to the fact that the GEM-FLEXPART simulation has no background tropospheric ozone.

The FLEXPART simulation also indicates that some stratospheric ozone reached the ground between April 29 and May 2. This is also evident in the ozonesonde profiles, particularly on May 2 at 0 UT.

Fig. 7 shows a similar comparison, of vertical profiles of measured ozone mixing ratio and values from a GEM-FLEXPART simulation, for the February 2007 Walsingham campaign. In this case FLEXPART modeling suggests that little stratospheric ozone reached the ground. However the similarity, although less than perfect, is again obvious, and indicates that much of the observed variability of ozone in the upper troposphere is due to the stratospheric source. A quantitative comparison (Table 2) indicates that STT, while highly variable, is responsible for an average, over the seven campaigns, of 34% (22 ppb) of the ozone in the middle and upper troposphere (3–8 km). These results are averages from each 10-day FLEXPART run, initialized with the average value of measured stratospheric ozone over each campaign period, and compared with the corresponding measurements of tropospheric ozone by the ozonesondes.

Although the campaigns were organized to provide data for different seasons, it is, unfortunately, difficult to discern a clear seasonal pattern in the amount of ozone injected into the troposphere. Although frequent intrusion events were observed in the spring and summer campaigns, the largest amounts of ozone transported into the troposphere were in fall and winter, and in the summer campaign at Harrow. With one exception, all showed significant amounts of stratospheric ozone in the 3–8 km layer, and in that case (the August 2006 campaign at Walsingham) large amounts of ozone were found, by both sondes and FLEXPART, below the tropopause but above 8 km. However, only three campaigns show significant amounts of stratospheric ozone in the 0–1 km layer; one in late fall, one in spring and one in summer. Averaged over all seven campaigns, 3.1% of boundary layer ozone (1.2 ppb), and 13% of ozone in the lower troposphere (5.4 ppb) was of stratospheric origin, where these layers are defined as 0–1 km, and 1–3 km respectively.

### 5.2. IONS and BORTAS campaigns

Layers of apparent stratospheric origin can also be recognized in ozonesonde profiles, as for example in Fig. 3 (left), over Montreal on May 5, 2005, where a layer of high ozone between 4 and 6 km is evident, strongly anticorrelated with relative humidity (RH). The relative humidity/$O_3$ relationship is frequently used as a simple indicator of probable stratospheric origin (e.g. Van Haver et al., 1996; Newell et al., 1999; Stohl et al., 2000; Cristofanelli et al., 2006; Bourqui et al., 2012; Vérèmes et al., 2016). It is most effective for layers of recent stratospheric origin (Trickl et al., 2010; Stohl et al., 2000; Appenzeller et al., 1996), but in many cases layers can persist much longer (Trickl et al., 2014, 2016; Osman et al., 2016). This indicator was applied to the

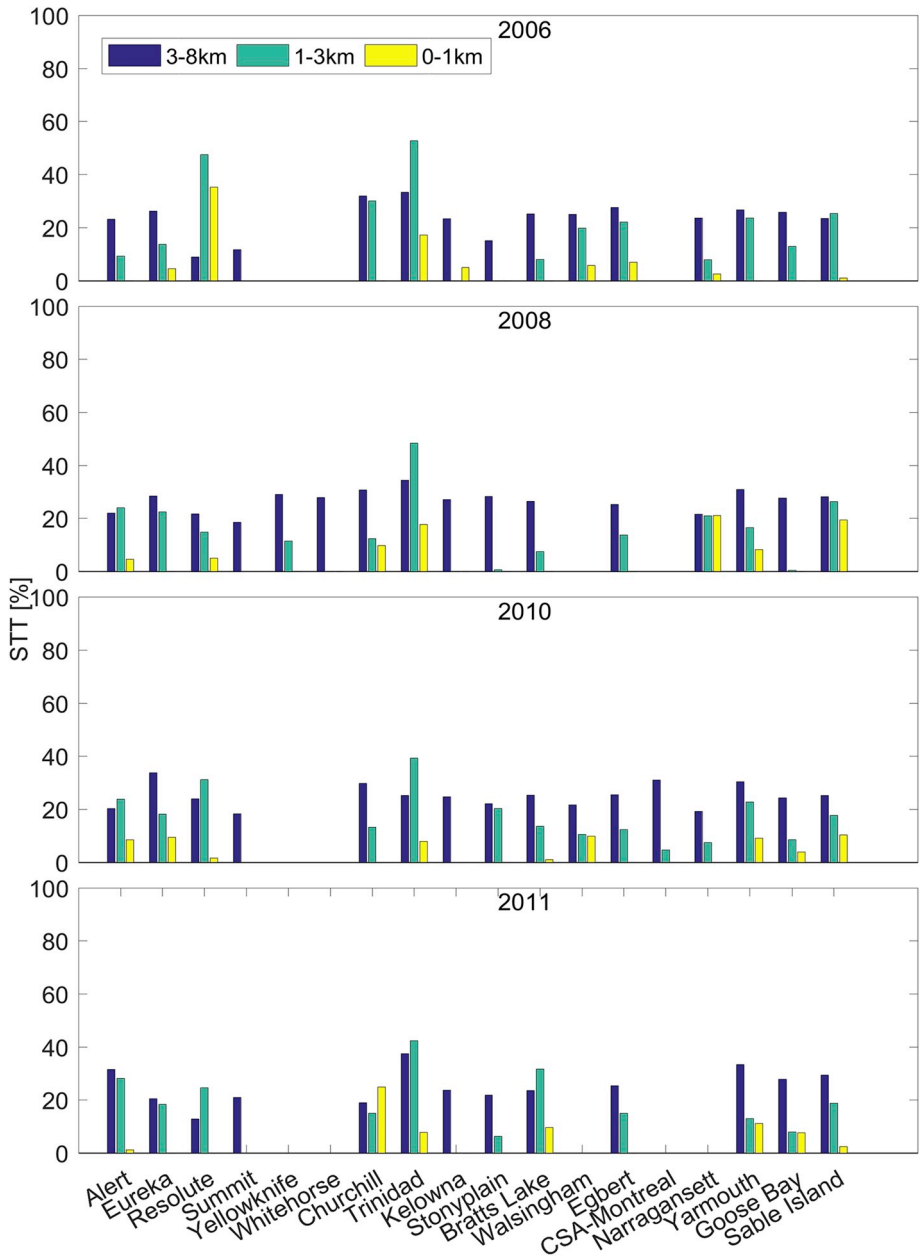


**Fig. 9.** Estimated contribution of stratosphere-troposphere transport (STT) to ozone in the boundary layer (0–1 km), the lower troposphere (1–3 km) and the middle and upper troposphere (3–8 km), during the four summertime field campaigns described in Table 1, using the ozone-RH correlation algorithm described in Section 5.2.

ozonesonde profiles of the radar-ozonesonde campaigns in Table 2, and subsequently to those in Table 1, in three steps, applied to each profile individually:

1. A smoothed profile was obtained by boxcar averaging the high-resolution profile to remove variations of vertical half-width less than 1.5 km. The difference of the high-resolution profile and the smoothed profile, divided by the smoothed profile, was defined as the normalized perturbation profile.
2. The same method was used to determine a normalized perturbation profile of RH. Boxcar averaging to filter out variations of vertical half-width less than 5 km was used to create the RH smoothed profile.
3. Ozone laminae in the normalized perturbation profile with average amplitudes greater than 0.05 were considered significant if coincident with negative RH laminae with average amplitudes greater than 0.25; that is, ozone perturbations greater than 5%, coincident with decreases in RH of more than 25%.

An example is shown in Fig. 8. Suspected stratospheric layers were detected by this method in most profiles, which seems consistent with the comparisons in Figs. 6 and 7, and with the previously noted observation (Section 4) that intrusion events typically occur every 2–3 days in spring and summer. The number of layers detected, and therefore the amount of stratospheric ozone in the troposphere estimated by this method is somewhat dependent on the choice of parameters in steps 1–3 above (Van Haver et al., 1996; Newell et al., 1999). As a sensitivity test, these were varied, and compared to the results of the FLEXPART calculation in Table 2. As expected, varying the ozone perturbation threshold produced a corresponding change in the amount of stratospheric ozone detected (at all levels), and broader smoothing of the mean ozone profile produced larger perturbations and therefore

**Table 3**
Percentage contribution of stratospheric ozone to the total tropospheric ozone column (TTOC), and to three defined layers in the troposphere, as calculated by the RH/$O_3$ relationship, using ozonesonde data from the four field campaigns described in Table 1. Station locations are shown in Fig. 1.

| Site Name | TTOC | 0-1 km | 1-3 km | 3-8 km |
|---|---|---|---|---|
| Alert | 20.0 | 3.6 | 21.3 | 24.3 |
| Eureka | 20.3 | 3.5 | 18.2 | 27.3 |
| Resolute | 17.6 | 10.5 | 29.5 | 16.9 |
| Summit | 14.2 | – | – | 17.4 |
| Yellowknife | 21.7 | 0.0 | 11.5 | 29.1 |
| Whitehorse | 16.5 | 0.0 | 0.0 | 27.9 |
| Churchill | 21.5 | 8.7 | 17.7 | 27.9 |
| Trinidad Head | 30.4 | 12.7 | 45.7 | 32.6 |
| Kelowna | 16.2 | 1.2 | 0.0 | 24.7 |
| Stonyplain | 15.3 | 0.0 | 6.8 | 21.9 |
| Bratt's Lake | 20.5 | 2.7 | 15.2 | 25.1 |
| Walsingham | 19.2 | 7.9 | 15.2 | 23.3 |
| Egbert | 19.4 | 1.7 | 15.8 | 25.9 |
| CSA-Montreal | 19.6 | 0.0 | 4.7 | 31.1 |
| Narragansett | 16.8 | 7.9 | 12.1 | 21.5 |
| Yarmouth | 22.4 | 7.1 | 19.0 | 30.4 |
| Goose Bay | 17.9 | 2.9 | 7.4 | 26.4 |
| Sable Island | 21.1 | 8.4 | 22.1 | 26.6 |
| Mean | 19.5 | 4.6 | 15.4 | 25.6 |

more STT. In contrast, lowering the relative humidity perturbation threshold had little effect on the amount of stratospheric ozone in the upper troposphere, but a large effect on STT detected in the lowest kilometre. The different results obtained from varying the threshold parameters correlated well with each other, but none showed a significant correlation with the FLEXPART results. This is disappointing, and suggests caution in use of this simple method. The FLEXPART results also show a much larger variance. The parameters described above were chosen to yield the best match to the FLEXPART results.

The agreement, as can be seen from Table 2, is not very good: while the estimated STT magnitudes are similar on average – 23%, 18% and 4.8%, versus 34%, 13% and 3.1% – those for individual campaigns show little correlation. The reasons for this are likely several: FLEXPART uses 10-day trajectories, while the RH-$O_3$ anticorrelation is observed to decay after 3–4 days (Stohl et al., 2000; Appenzeller et al., 1996); the anticorrelation of RH and $O_3$ in a layer can be produced by simple descent from the upper troposphere where the absolute humidity is much lower, and so it is not a definite indicator of stratospheric origin; and intrusions are small-scale, highly variable dynamic phenomena, and so a 1-D time series like the sonde or FLEXPART curtains of Figs. 6 and 7 may miss features (e.g. Fig. 2; see also the discussion in Langford et al., 2009). Small trajectory errors can therefore lead to large differences in such 1-D time series, and in fact typical trajectory errors are 100–200 km day$^{-1}$ (Stohl, 1998). For these reasons the correspondence of the left and right-hand plots in Figs. 6 and 7 is also less than perfect. Nevertheless, assuming that trajectory errors are random, the similarity in average estimated STT magnitudes suggests that this method may produce reasonable aggregate results (e.g. Newell et al., 1999; Stohl et al., 2000).

The RH-$O_3$ algorithm was then applied to the large set of ozonesonde profiles from the IONS and BORTAS campaigns (Table 1). The total STT contribution calculated by this method varies from about 2 to 12 Dobson units (DU), but its variability as a fraction of the total tropospheric ozone column (TTOC) between sites and years is fairly modest (Fig. 9), ranging from a minimum of 14% (at Summit) to a maximum of 30% (at Trinidad Head). No pattern is apparent to the variability between years. There is more ozone, in DU, attributable to STT at the sites further east and south, but these are also sites with larger tropospheric columns, and so as a percentage of TTOC the variability between sites is rather small (Table 3). Intersite variability may depend on geography: while a large contribution is found at

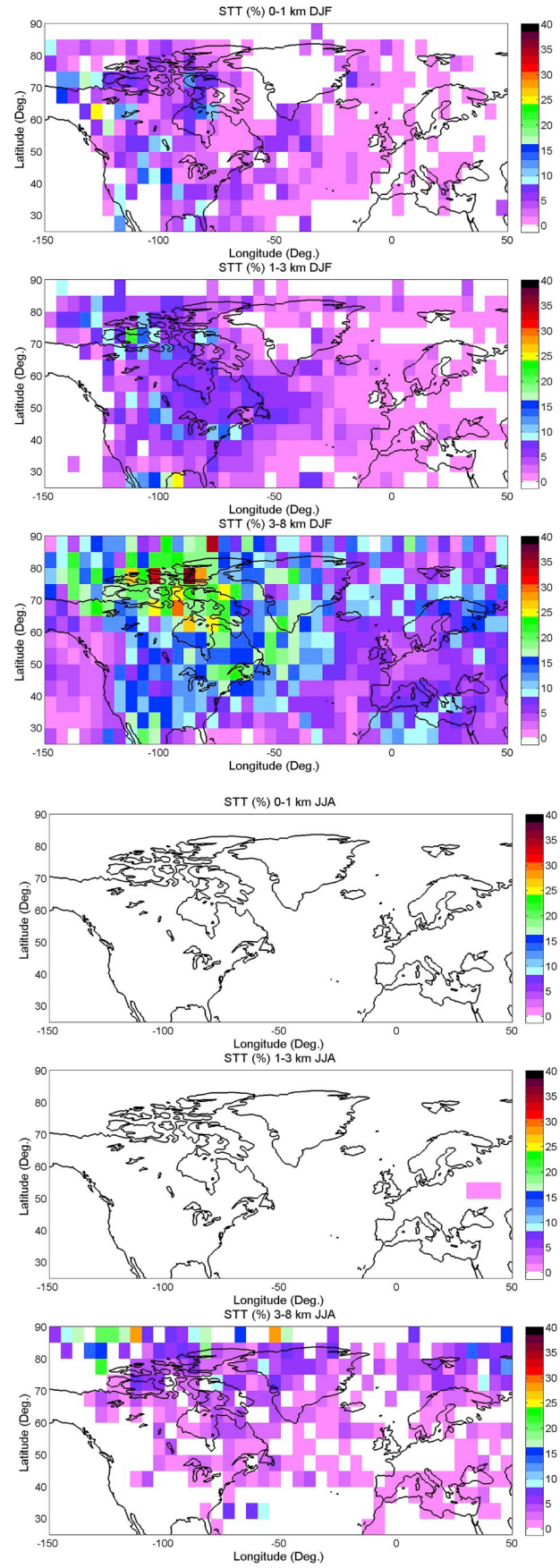


*(caption on next page)*

**Fig. 10.** Estimated contribution of rapid stratosphere-troposphere transport, to three defined layers in the troposphere, based on trajectories up to 4 days in length launched from the locations of ozone soundings (all profiles, 1990–1999). The region displayed (25–90 N and 50 E to 150 W) is selected because of the relatively high density of sonde data (see Liu et al., 2013b, Fig. 14, or Tarasick et al., 2018, Fig. 16). The seasonality is marked, with the maximum contributions in winter (DJF) and spring (MAM), and the minimum in summer (JJA).

Trinidad Head, the Kelowna site, also on the west coast, shows about half this much (16%). Kelowna is situated between mountain ranges. Elbern et al. (1997) similarly found STT to be less frequent in a mountain valley.

Table 3 also shows the contribution of STT to ozone in the three tropospheric layers defined in Table 2. As for the short campaigns in Table 2, the calculated contribution in the lower troposphere and the boundary layer is highly variable between sites. However, it is much less variable in the 3–8 km layer. The mean fractions over all sites are 4.6% of boundary layer ozone, 15% of ozone in the lower troposphere, and 26% in the middle and upper troposphere.

### 5.3. Estimates based on HYSPLIT trajectories (TOST)

The TOST ozone data product offers an additional way to estimate ozone cross-tropopause transport, on a global domain, using ozone soundings and forward trajectories from the sonde locations above the tropopause. For each TOST 5 × 5 degree x 1 km bin, the number of trajectories starting in the stratosphere, weighted by their average ozone concentration, is divided by the total number of trajectories from both stratospheric and tropospheric sources contributing to that bin, weighted by their average ozone concentration. Individual 1-km bins are summed vertically to produce the 1–3 km and 3–8 km columns. The trajectories in TOST are all launched from ozonesonde locations, so there is some risk of sampling bias (primarily gaps), as the sounding locations are not evenly distributed globally. Fortunately the random character of trajectories ensures excellent global coverage (Liu et al., 2013a), over the decade of the 1990s employed here. Additionally, the results presented here are restricted to the region 25–90 N and 50 E to 150 W, because of the relatively high density of sonde data there (see Liu et al., 2013b, Fig. 14, or Tarasick et al., 2018, Fig. 16).

Fig. 10 shows the estimated contribution of rapid stratosphere-troposphere transport, to the previously defined three layers in the troposphere, based on TOST trajectories (up to 4 days in length, launched from the locations of ozonesonde profiles). Several features are apparent from these figures:

(1) While much more ozone of stratospheric origin is found in the middle and upper troposphere, significant amounts also reach the lowest kilometre (i.e. the boundary layer). Since the TOST trajectories are a maximum of 4 days in length, this presumably represents deep, irreversible transport;
(2) STT is much stronger in North America than Europe. This is somewhat surprising, and not likely due to sampling artifacts, as the frequency of soundings is greater in Europe than North America. This pattern is also reflected in maps presented by Škerlak et al. (2014);
(3) The STT flux of ozone is much larger in winter (DJF) and spring (MAM), than in summer (JJA) or autumn (SON). This is consistent with previous observations that STT exerts the largest influence on surface ozone in the spring (Danielsen and Mohnen, 1977; Holton et al., 1995; Monks, 2000), but seems to differ from the results of the radar-ozonesonde campaigns discussed in Section 4, which showed more STT events in summer than winter. The difference is likely explained by the fact that there is more ozone in the lowermost stratosphere during winter;
(4) There is an evident tendency for high values to appear north of 60N, but this is really only true in the middle/upper tropospheric layer, and is likely due to the lower tropopause in polar regions. In addition, some of these trajectories may return to the stratosphere (Stohl et al., 2003a).

Table 4 averages these STT contributions over several latitude bands, restricting the area of interest to the North American continent (125W–50W). Over this region the average magnitudes are closer to those found by the other methods, but while remaining in approximately the same proportions, they are quite variable, and on average about 3–4 times smaller. This may be because the TOST trajectories are limited to 4 days (and so represent only rapid STT) and/or because of the coarse vertical resolution (1 km) of the TOST trajectories, and the corresponding tropopause (since stratospheric intrusions generally originate close to the tropopause).

## 6. Conclusions

Twice daily ozonesondes were launched during seven 10-day campaigns, incorporating nearby windprofiler measurements, in Ontario and Quebec between 2005 and 2007. Numerous stratosphere-troposphere transport events were observed, demonstrating a strong relationship between rapid increases in the radar-determined tropopause height and stratospheric intrusions. GEM-FLEXPART modeling is able to reproduce much of the observed variability of ozone in the upper troposphere, confirming its stratospheric origin, and also indicating that the Canadian operational forecast model, GEM, is representing upper tropospheric dynamics quite well.

Further examination shows that where the radar-determined tropopause differs from the WMO thermal tropopause, the radar is typically responding to the sharp gradients of potential temperature and humidity at the lower edge of a stratospheric intrusion. Radar appears to be a particularly good intrusion detector. In addition to explaining the radar's success at finding STE events, this fact can potentially be used to follow the descent of layers of stratospheric origin in the troposphere. Windprofilers can routinely and continuously measure the height of the tropopause, and so it seems likely that the assimilation of inexpensive windprofiler data would lead to improvement in tropospheric dynamical and air quality forecasts.

The ability of FLEXPART to reproduce the pattern of variability observed in the radar-ozonesonde campaigns, although less than perfect, lends confidence to further calculations. By initializing 10-day GEM-FLEXPART runs with the average value of measured stratospheric ozone during each campaign, it was possible to make a realistic estimate of the amount of ozone transported into the troposphere, and its contribution relative to the corresponding measurements by the ozonesondes. These estimates differ widely between campaigns, in part because they were undertaken in different seasons and at different sites, but primarily because of the sporadic nature of STT. On the assumption that these variations are random, the FLEXPART results were used to calibrate the adjustable parameters in a calculation using the relative humidity – ozone anticorrelation, which was then extended to a much larger set of ozone soundings from several campaigns at 18 sites in North America.

The FLEXPART calculations indicated that STT contributed an average, over the seven radar-ozonesonde campaigns, of 3.1% (1.2 ppb) of ozone in the boundary layer (0–1 km), but 13% (5.4 ppb) in the lower troposphere (1–3 km) and 34% (22 ppb) in the middle and upper troposphere (3–8 km). The RH-$O_3$ calculation, applied to four summertime campaigns at a large set of sites, estimated STT to be responsible for 4.6% of boundary layer ozone, 15% of ozone in the lower troposphere, and 26% in the middle and upper troposphere.

STT calculations were also performed using the TOST global 3D trajectory-mapped ozone data product, for four seasons. The resulting maps indicate that STT is stronger over the North American continent than Europe, and much stronger in winter and spring than in summer or

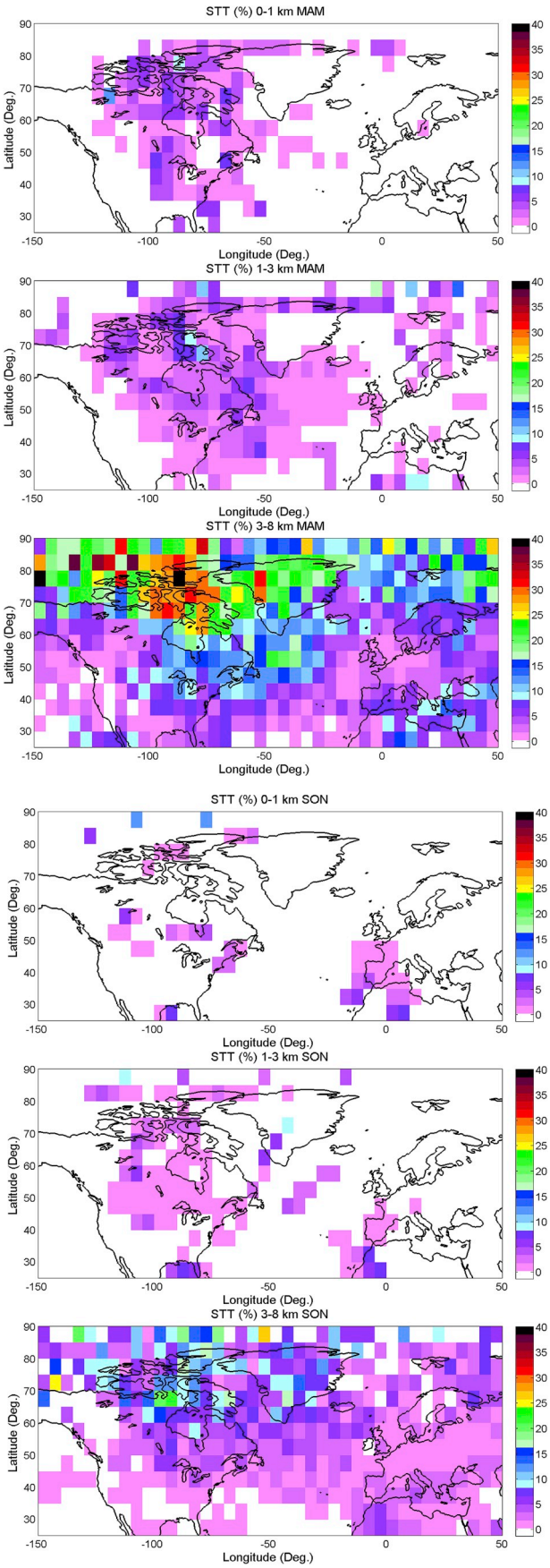


**Fig. 10.** (*continued*)

**Table 4**
Stratospheric contribution in per cent to ozone in three defined layers in the troposphere, for North America (125W–50W), in three latitude bands, as calculated by the HYSPLIT-based method described in Section 5.3.

| STT (%) NA | DJF | MAM | JJA | SON |
|---|---|---|---|---|
| 25–40N | | | | |
| *0-1 km* | 3.5 | 1.0 | 0 | 0.2 |
| *1-3 km* | 4.9 | 0.8 | 0 | 0.5 |
| *3-8 km* | 8.2 | 3.9 | 0.6 | 0.4 |
| 40–60N | | | | |
| *0-1 km* | 3.8 | 1.4 | 0 | 0.5 |
| *1-3 km* | 6.2 | 2.4 | 0 | 0.8 |
| *3-8 km* | 12.6 | 8.3 | 1.2 | 2.8 |
| 60–90N | | | | |
| *0-1 km* | 2.7 | 2.2 | 0 | 0.4 |
| *1-3 km* | 4.5 | 2.9 | 0 | 0.8 |
| *3-8 km* | 17.1 | 21.1 | 4.4 | 8.1 |

fall. Average overall magnitudes are 3–4 times smaller than expected from the previous calculations, at all levels. This may be because the TOST trajectories are limited to 4 days (and so represent only rapid STT) and/or because of the coarse vertical resolution (1 km) of the TOST trajectories.

The TOST-based STT estimate could be improved, in a dedicated calculation, by increasing the vertical density of trajectories near the tropopause and a more precise tropopause definition, as stratospheric intrusions generally originate close to the tropopause. The use of longer (e.g. 10-day) trajectories might also produce estimates closer in average magnitude to the FLEXPART campaign results. The implied increase in computational cost is significant, however. Both the TOST-based and the RH-$O_3$ estimates can be extended to the global ozonesonde record, which is now more than 50 years in length at some sites. Estimates of trends in the magnitude of STT over that period would be of interest. The RH-$O_3$ calculation has the advantage of being independent of model and data assimilation changes, although not of possible radiosonde RH-sensor changes.

## Acknowledgements

This work was funded primarily by the Canadian Foundation for Climate and Atmospheric Science, and by the Natural Sciences and Engineering Research Council of Canada. The McGill and Walsingham radars were installed with support from the Canadian Foundation for Innovation. Funding of the IONS ozonesondes was provided by Environment Canada; NOAA; NASA; U.S. EPA; Max Plank Institute for Chemistry, Mainz; Los Alamos National Laboratory; Valparaiso University; the University of Rhode Island; the California Department of Energy; the California Air Resources Board; and the Friends of the Green Horse Society via a grant from ExxonMobil Canada. The authors acknowledge valuable conversations with Owen Cooper of the University of Colorado/NOAA Earth System Research Laboratory,. Valuable technical support was provided by Gwyneth Carey-Smith, Jonathan Davies, Tim Officer, Mark van der Zanden and Ryan van der Zanden. The use of facilities at the Canadian Space Agency in Montreal was made possible with help from Stella Melo, Ron Wilkinson and Réjean Michaud. TOST data were obtained from the World Ozone and Ultraviolet Radiation Data Center (WOUDC) operated by Environment and Climate Change Canada, Toronto, Ontario, Canada, under the auspices of the World Meteorological Organization.

## Appendix A. Supplementary data

Supplementary data to this article can be found online at https://doi.org/10.1016/j.atmosenv.2018.10.040.

## References


Akritidis, D., Pozzer, A., Zanis, P., Tyrlis, E., Škerlak, B., Sprenger, M., Lelieveld, J., 2016. On the role of tropopause folds in summertime tropospheric ozone over the eastern Mediterranean and the Middle East. Atmos. Chem. Phys. 16, 14025–14039. https://doi.org/10.5194/acp-16-14025-2016.

Appenzeller, C., Davies, H.C., Norton, W.A., 1996. Fragmentation of stratospheric intrusions. J. Geophys. Res. 101 (D1), 1435–1456. https://doi.org/10.1029/95JD02674.

Avnery, S., Mauzerall, D.L., Liu, J., Horowitz, L.W., 2011. Global crop yield reductions due to surface ozone exposure: 1. Year 2000 crop production losses and economic damage. Atmos. Environ. 45, 2284–2296. https://doi.org/10.1016/j.atmosenv.2011.01.002.

Bachmeier, E.V., Shipman, M.C., Browell, E.V., Grant, W.B., Klassa, J.M., 1994. Stratospheric/tropospheric exchange affecting the northern wetlands regions of Canada during summer 1990. J. Geophys. Res. 99, 1793–1804.

Banerjee, A., Maycock, A.C., Archibald, A.T., Abraham, N.L., Telford, P., Braesicke, P., Pyle, J.A., 2016. Drivers of changes in stratospheric and tropospheric ozone between year 2000 and 2100. Atmos. Chem. Phys. 16, 2727–2746. https://doi.org/10.5194/acp-16-2727-2016.

Bell, M.L., Zanobetti, A., Dominici, F., 2014. Who is more affected by ozone pollution? A systematic review and meta-analysis. Am. J. Epidemiol. 180, 15–28. https://doi.org/10.1093/aje/kwu115.

Bourqui, M.S., Trépanier, P.-Y., 2010. Descent of deep stratospheric intrusions during the IONS August 2006 campaign. J. Geophys. Res. 115, D18301. https://doi.org/10.1029/2009JD013183.

Bourqui, M., Yamamoto, A., Tarasick, D., Moran, M.D., Beaudoin, L.-P., Beres, I., Davies, J., Elford, A., Hocking, W., Osman, M., Wilkinson, R., 2012. A new real-time Lagrangian diagnostic system for stratosphere-troposphere exchange: evaluation during a balloon sonde campaign in eastern Canada. Atmos. Chem. Phys. 12, 2661–2679. https://doi.org/10.5194/acp-12-2661-2012.

Butchart, N., 2014. The Brewer-Dobson circulation. Rev. Geophys. 52. https://doi.org/10.1002/2013RG000448.

Butchart, N., Scaife, A.A., Bourqui, M., de Grandpré, J., Hare, S.H.E., Kettleborough, J., Langematz, U., Manzini, E., Sassi, F., Shibata, K., Shindell, D., Sigmond, M., 2006. Simulations of anthropogenic change in the strength of the Brewer-Dobson circulation. Clim. Dyn. 27, 727–741. https://doi.org/10.1007/s00382-006-0162-4.

Calvert, J.G., Orlando, J.J., Stockwell, W.R., Wallington, T.J., 2015. The Mechanisms of Reactions Influencing Atmospheric Ozone. Oxford University Press, New York, pp. 590.

Chung, Y.S., Dann, T., 1985. Observation of stratospheric ozone at the ground level in Regina, Canada, *Atmos*. Environ. Times 19, 157–162. https://doi.org/10.1016/0004-6981(85)90147-7.

Colette, A., Ancellet, G., 2005. Impact of vertical transport processes on the tropospheric ozone layering above Europe. Part II: climatological analysis of the past 30 years. Atmos. Environ. 39 (29), 5423–5435. https://doi.org/10.1016/j.atmosenv.2005.06.015.

Cooper, O.R., Moody, J.L., 2000. Meteorological controls on ozone at an elevated eastern United States regional background monitoring site. J. Geophys. Res. 105, 6855–6869.

Cooper, O.R., Stohl, A., Hübler, G., Hsie, E.Y., Parrish, D.D., Tuck, A.F., Kiladis, G.N., Oltmans, S.J., Johnson, B.J., Shapiro, M., Moody, J.L., Lefohn, A.S., 2005. Direct transport of mid-latitude stratospheric ozone into the lower troposphere and marine boundary layer of the tropical Pacific Ocean. J. Geophys. Res. 110, D23310. https://doi.org/10.1029/2005JD005783.

Cooper, O.R., Stohl, A., Trainer, M., Thompson, A., Witte, J.C., Oltmans, S.J., Morris, G., Pickering, K.E., Crawford, J.H., Gao Chen, Cohen, R.C., Bertram, T.H., Wooldridge, P., Perring, A., Brune, W.H., Merrill, J., Moody, J.L., Tarasick, D., Nédélec, P., Forbes, G., Newchurch, M.J., Schmidlin, F.J., Johnson, B.J., Turquety, S., Baughcum, S.L., Ren, X., Fehsenfeld, F.C., Meagher, J.F., Spichtinger, N., Brown, C.C., McKeen, S.A., McDermid, I.S., Leblanc, T., 2006. Large upper tropospheric ozone enhancements above mid-latitude North America during summer: in situ evidence from the IONS and MOZAIC ozone measurement network. J. Geophys. Res. 111, D24S05. https://doi.org/10.1029/2006JD007306.

Cooper, O.R., Oltmans, S.J., Johnson, B.J., Brioude, J., Angevine, W., Trainer, M., Parrish, D.D., Ryerson, T.R., Pollack, I., Cullis, P.D., Ives, M.A., Tarasick, D.W., Al-Saadi, J., Stajner, I., 2011. Measurement of western U.S. baseline ozone from the surface to the tropopause and assessment of downwind impact regions. J. Geophys. Res. 116, D00V03. https://doi.org/10.1029/2011JD016095.

Cristofanelli, P., Bonasoni, P., Tositti, L., Bonafe, U., Calzolari, F., Evangelisti, F., Sandrini, S., Stohl, A., 2006. A 6-year analysis of stratospheric intrusions and their influence on ozone at Mt. Cimone (2165 m above sea level). J. Geophys. Res. 111, D03306. https://doi.org/10.1029/2005JD006553.

Cristofanelli, P., Bracci, A., Sprenger, M., Marinoni, A., Bonafè, U., Calzolari, F., Duchi, R., Laj, P., Pichon, J.M., Roccato, F., Venzac, H., Vuillermoz, E., Bonasoni, P., 2010. Tropospheric ozone variations at the Nepal Climate Observatory-Pyramid (Himalayas, 5079 m a.s.l.) and influence of deep stratospheric intrusion events. Atmos. Chem. Phys. 10, 6537–6549. https://doi.org/10.5194/acp-10-6537-2010.

Danielsen, E.F., 1968. Stratospheric-tropospheric exchange based on radioactivity, ozone and potential vorticity. J. Atmos. Sci. 25, 502–518.

Danielsen, E.F., Mohnen, V.A., 1977. Project dustorm report: ozone transport, in situ measurements, and meteorological analyses of tropopause folding. J. Geophys. Res. 82 (37), 5867–5877. https://doi.org/10.1029/JC082i037p05867.

Davies, T.D., Schuepbach, E., 1994. Episodes of high ozone concentrations at the earth's surface resulting from transport down from the upper troposphere/lower stratosphere: a review and case studies. Atmos. Environ. 28 (1), 53–68.

Dempsey, F., 2014. Observations of stratospheric $O_3$ intrusions in air quality monitoring data in Ontario, Canada. Atmos. Environ. 98, 111–122. https://doi.org/10.1016/j.atmosenv.2014.08.024.

Dibb, J.E., Meeker, L.D., Finkel, R.C., Southon, J.R., Caffee, M.W., Barrie, L.A., 1994. Estimation of stratospheric input to the Arctic troposphere: $^{7}$Be and $^{10}$Be aerosols at Alert, Canada. J. Geophys. Res. 99 (12) 855–12,864.

Dibb, J.E., Talbot, R.W., Scheuer, E., Seid, G., DeBell, L., Lefer, B.L., Ridley, B., 2003. Stratospheric influence on the northern North American free troposphere during TOPSE: $^{7}$Be as a stratospheric tracer. J. Geophys. Res. 108 (D4), 8363. https://doi.org/10.1029/2001JD001347.

Draxler, R.R., Hess, G.D., 1998. An overview of the HYSPLIT_4 modelling system for trajectories, dispersion, and deposition. Aust. Meteorol. Mag. 47, 295–308.

Eisele, H., Scheel, H.E., Sladkovic, R., Trickl, T., 1999. High-resolution lidar measurements of stratosphere-troposphere exchange. J. Atmos. Sci. 56, 319–330.

Elbern, H., Kowol, J., Sladkovic, R., Ebel, A., 1997. Deep stratospheric intrusions: a statistical assessment with model guided analysis. Atmos. Environ. 31 (No. 19), 3207–3226.

Fabian, P., Pruchniewicz, P.G., 1977. Meridional distribution of ozone in the troposphere and its seasonal variation. J. Geophy. Res. 82, 2063–2073.

Fusco, A.C., Logan, J.A., 2003. Analysis of 1970-1995 trends in tropospheric ozone at Northern Hemisphere midlatitudes with the GEOS-Chem model. J. Geophys. Res. 108 (D15), 4449.

He, H., Tarasick, D.W., Hocking, W.K., Carey-Smith, T.K., Rochon, Y., Zhang, J., Makar, P.A., Osman, M., Brook, J., Moran, M., Jones, D., Mihele, C., Wei, J.C., Osterman, G., Argall, P.S., McConnell, J., Bourqui, M.S., 2011. Transport analysis of ozone enhancement in southern Ontario during BAQS-met. Atmos. Chem. Phys. 11, 2569–2583. https://doi.org/10.5194/acp-11-2569-2011.

Hess, P.G., Zbinden, R., 2013. Stratospheric impact on tropospheric ozone variability and trends: 1990-2009. Atmos. Chem. Phys. 13, 649–674.

Hocking, W.K., 1997. System design, signal-processing procedures, and preliminary results for the Canadian (London, Ontario) VHF atmospheric radar. Radio Sci. 32 (2), 687–706. https://doi.org/10.1029/96RS03316.

Hocking, W.K., Carey-Smith, T.K., Tarasick, D.W., Argall, P.S., Strong, K., Rochon, Y., Zawadzki, I., Taylor, P.A., 2007. Detection of stratospheric ozone intrusions by windprofiler radars. Nature 450 (7167), 281–284. https://doi.org/10.1038/nature06312.

Holton, J.R., Haynes, P.H., Mcintyre, M.E., Douglass, A.R., Rood, B., 1995. Stratosphere-troposphere exchange. Rev. Geophys. 33 (4), 403–439.

Hooper, D.A., Arvelius, J., 2000. Monitoring of the Arctic winter tropopause: a comparison of radiosonde, ozonesonde and MST radar observations. In: Edwards, B. (Ed.), Proceedings of the Ninth International Workshop on Technical and Scientific Aspects of MST Radar Combined with COST76 Final Profiler Workshop, pp. 385–388 Sci. Comm. On Sol.-Terr. Phys. Secr. and Météo-France, Boulder, Colorado, 2000.

IPCC, 2001. Climate Change 2001, the Physical Science Basis, Working Group I, Chapter 6, Section 6.5.2.1, Ozone Radiative Forcing: Process Studies.

IPCC, 2013. Climate Change 2013 – Contribution of Working Group 1 to the Fifth Assessment Report of the Intergovernmental Panel on *Climate Change: the Physical Science Basis*. Cambridge University Press, Cambridge, United Kingdom and New York, NY, USA.

Jerrett, M., Burnett, R.T., Pope III, C.A., Ito, K., Thurston, G., Krewski, D., Shi, Y., Calle, E., Thun, M., 2009. Long-term ozone exposure and mortality. N. Engl. J. Med. 360, 1085–1095.

Johnson, W.B., Viezee, W., 1981. Stratospheric ozone in the lower troposphere. Presentation and interpretation of aircraft measurements. Atmos. Environ. 15, 1309–1323. https://doi.org/10.1016/0004-6981(81)90325-5.

Junge, C.E., 1962. Global ozone budget and exchange between stratosphere and troposphere. Tellus 14, 363–377.

Knowland, K.E., Ott, L.E., Duncan, B.N., Wargan, K., 2017. Stratospheric intrusion-influenced ozone air quality exceedances investigated in the NASA MERRA-2 reanalysis. Geophys. Res. Lett. 44 (10) 691–10,701. https://doi.org/10.1002/2017GL074532.

Langford, A.O., Aikin, K.C., Eubank, C.S., Williams, E.J., 2009. Stratospheric contribution to high surface ozone in Colorado during springtime. Geophys. Res. Lett. 36. https://doi.org/10.1029/2009GL038367.

Langford, A.O., Brioude, J., Cooper, O.R., Senff, C.J., Alvarez II, R.J., Hardesty, R.M., Johnson, B.J., Oltmans, S.J., 2012. Stratospheric influence on surface ozone in the Los Angeles area during late spring and early summer of 2010. J. Geophys. Res. 117, D00V06. https://doi.org/10.1029/2011JD016766.

Langford, A.O., Alvarez, J., Brioude, J., Evan, S., Iraci, T., Kirgis, G., Kuang, S., Leblanc, T., Newchurch, M.J., Pierce, R.B., Senff, C.J., Yates, E.L., 2018. Coordinated profiling of stratospheric intrusions and transported pollution by the tropospheric ozone lidar network (TOLNet) and NASA alpha jet experiment (AJAX): observations and comparison to HYSPLIT, RAQMS, and FLEXPART. Atmos. Environ. 174, 1–14. https://doi.org/10.1016/j.atmosenv.2017.11.031.

Lefohn, A., Emery, C., Shadwick, D., Wernli, H., Jung, J., Oltmans, S., 2014. Estimates of background surface ozone concentrations in the United States based on model-derived source apportionment. Atmos. Environ. 84, 275–288. https://doi.org/10.1016/j.atmosenv.2013.11.033.

Lin, M., Fiore, A.M., Cooper, O.R., Horowitz, L.W., Langford, A.O., Levy II, H., Johnson, B.J., Naik, V., Oltmans, S.J., Senff, C.J., 2012. Springtime high surface ozone events over the western United States: quantifying the role of stratospheric intrusions. J. Geophys. Res. 117, D00V22. https://doi.org/10.1029/2012JD018151.

Liu, G., Liu, J.J., Tarasick, D.W., Fioletov, V.E., Jin, J.J., Moeni, O., Liu, X., Sioris, C.E., Osman, M., 2013a. A global tropospheric ozone climatology from trajectory-mapped ozone soundings. Atmos. Chem. Phys. 13, 10659–10675. https://doi.org/10.5194/acp-13-10659-2013.

Liu, J., Tarasick, D.W., Fioletov, V.E., McLinden, C., Zhao, T., Gong, S., Sioris, C., Jin, J., Liu, G., Moeini, O., 2013b. A global ozone climatology from ozone soundings via trajectory mapping: a stratospheric perspective. Atmos. Chem. Phys. 13, 11441–11464. https://doi.org/10.5194/acp-13-11441-2013.

McGrath, J.M., Betzelberger, A.M., Wang, S., Shook, E., Zhu, X.-G., Long, S.P., Ainsworth, E.A., 2015. An analysis of ozone damage to historical maize and soybean yields in the United States. Proc. Natl. Acad. Sci. Unit. States Am. 112 (46), 14390–14395. https://doi.org/10.1073/pnas.1509777112.

Monks, P.S., 2000. A review of the observations and origins of the spring ozone maximum. Atmos. Environ. 34 (21), 3545–3561.

Neu, J.L., Flury, T., Manney, G.L., Santee, M.L., Livesey, N.J., Worden, J., 2014. Tropospheric ozone variations governed by changes in the stratospheric circulation. Nature Geosci 7, 340–344. https://doi.org/10.1038/NGEO2138.

Newell, R.E., Thouret, V., Cho, J.Y.N., Stoller, P., Marenco, A., Smit, H.G., 1999. Ubiquity of quasi horizontal layers in the troposphere. Nature 398, 316–319. https://doi.org/10.1038/18642.

Ordóñez, C., Brunner, D., Staehelin, J., Hadjinicolaou, P., Pyle, J.A., Jonas, M., Wernli, H., Prévôt, A.S.H., 2007. Strong influence of lowermost stratospheric ozone on lower tropospheric background ozone changes over Europe. Geophys. Res. Lett. 34, L07805. https://doi.org/10.1029/2006GL029113.

Osman, M.K., Hocking, W., Tarasick, D.W., 2016. Parameterization of large-scale turbulent diffusion in the presence of both well-mixed and weakly mixed patchy layers. J. Atmos. Solar-Terr. Phys. 143–144. 14-36. https://doi.org/10.1016/j.jastp.2016.02.025.

Palmer, P.I., Parrington, M., Lee, J.D., Lewis, A.C., Rickard, A.R., Bernath, P.F., Duck, T.J., Waugh, D.L., Tarasick, D.W., Andrews, S., Aruffo, E., Bailey, L.J., Barrett, E., Bauguitte, S.J.-B., Curry, K.R., Di Carlo, P., Chisholm, L., Dan, L., Forster, G., Franklin, J.E., Gibson, M.D., Griffin, D., Helmig, D., Hopkins, J.R., Hopper, J.T., Jenkin, M.E., Kindred, D., Kliever, J., Le Breton, M., Matthiesen, S., Maurice, M., Moller, S., Moore, D.P., Oram, D.E., O'Shea, S.J., Christopher Owen, R., Pagniello, C.M.L.S., Pawson, S., Percival, C.J., Pierce, J.R., Punjabi, S., Purvis, R.M., Remedios, J.J., Rotermund, K.M., Sakamoto, K.M., da Silva, A.M., Strawbridge, K.B., Strong, K., Taylor, J., Trigwell, R., Tereszchuk, K.A., Walker, K.A., Weaver, D., Whaley, C., Young, J.C., 2013. Quantifying the impact of BOReal forest fires on Tropospheric oxidants over the Atlantic using Aircraft and Satellites (BORTAS) experiment: design, execution and science overview. Atmos. Chem. Phys. 13, 6239–6261. https://doi.org/10.5194/acp-13-6239-2013.

Randel, W.J., Thompson, A.M., 2011. Interannual variability and trends in tropical ozone derived from SAGE II satellite data and SHADOZ ozonesondes. J. Geophys. Res. 116 (D07303), 1–9. https://doi.org/10.1029/2010JD015195.

Silva, R.A., West, J.J., Zhang, Y., Anenberg, S.C., Lamarque, J.-F., Shindell, D.T., Collins, W.J., Dalsoren, S., Faluvegi, G., Folberth, G., Horowitz, L.W., Nagashima, T., Naik, V., Rumbold, S., Skeie, R., Sudo, K., Takemura, T., Bergmann, D., Cameron-Smith, P., Cionni, I., Doherty, R.M., Eyring, V., Josse, B., MacKenzie, I.A., Plummer, D., Righi, M., Stevenson, D.S., Strode, S., Szopa, S., Zeng, G., 2013. Global premature mortality due to anthropogenic outdoor air pollution and the contribution of past climate change. Environ. Res. Lett. 8 (3), 034005. https://doi.org/10.1088/1748-9326/8/3/034005.

Sioris, C.E., McLinden, C.A., Fioletov, V.E., Adams, C., Zawodny, J.M., Bourassa, A.E., Roth, C.Z., Degenstein, D.A., 2014. Trend and variability in ozone in the tropical lower stratosphere over 2.5 solar cycles observed by SAGE II and OSIRIS. Atmos. Chem. Phys. 14, 3479–3496. https://doi.org/10.5194/acp-14-3479-2014.

Škerlak, B., Sprenger, M., Wernli, H., 2014. A global climatology of stratosphere-troposphere exchange using the ERA-interim dataset from 1979 to 2011. Atmos. Chem. Phys. 14, 913–937. https://doi.org/10.5194/acp-14-913-2014.

Smit, H.G.J., Straeter, W., Johnson, B., Oltmans, S., Davies, J., Tarasick, D.W., Hoegger, B., Stubi, R., Schmidlin, F., Northam, T., Thompson, A., Witte, J., Boyd, I., Posny, F., 2007. Assessment of the performance of ECC-ozonesondes under quasi-flight conditions in the environmental simulation chamber: insights from the Juelich ozone sonde intercomparison experiment (JOSIE). J. Geophys. Res. 112, D19306. https://doi.org/10.1029/2006JD007308.

Stevenson, D.S., Young, P.J., Naik, V., Lamarque, J.-F., Shindell, D.T., Voulgarakis, A., Skeie, R.B., Dalsoren, S.B., Myhre, G., Berntsen, T.K., Folberth, G.A., Rumbold, S.T., Collins, W.J., MacKenzie, I.A., Doherty, R.M., Zeng, G., van Noije, T.P.C., Strunk, A., Bergmann, D., Cameron-Smith, P., Plummer, D.A., Strode, S.A., Horowitz, L., Lee, Y.H., Szopa, S., Sudo, K., Nagashima, T., Josse, B., Cionni, I., Righi, M., Eyring, V., Conley, A., Bowman, K.W., Wild, O., 2013. Tropospheric ozone changes, radiative forcing and attribution to emissions in the atmospheric chemistry and climate model inter-comparison project (ACCMIP). Atmos. Chem. Phys. 13, 3063–3085. https://doi.org/10.5194/acp-13-3063-2013.

Stohl, A., 1998. Computation, accuracy and applications of trajectories - a review and bibliography. Atmos. Environ. 32, 947–966. https://doi.org/10.1016/S1352-2310(97)00457-3.

Stohl, A., Spichtinger-Rakowsky, N., Bonasoni, P., Feldmann, H., Memmesheimer, M., Scheel, H.E., Trickl, T., Hubener, S., Ringer, W., Mandl, M., 2000. The influence of stratospheric intrusions on alpine ozone concentrations. Atmos. Environ. 34, 1323–1354.

Stohl, A., et al., 2003a. Stratosphere-troposphere exchange: a review and what we have learned from STACCATO. J. Geophys. Res. 108, 8516. https://doi.org/10.1029/2002JD002490, 108(D12).

Stohl, A., Wernli, H., James, P., Bourqui, M., Forster, C., Liniger, M.A., Seibert, P., Sprenger, M., 2003b. A new perspective of stratosphere–troposphere exchange. Bull. Amer. Meteor. Soc. 84, 1565–1573. https://doi.org/10.1175/BAMS-84-11-1565.

Stohl, A., Forster, C., Frank, A., Seibert, P., Wotawa, G., 2005. Technical note: the Lagrangian particle dispersion model FLEXPART version 6.2. Atmos. Chem. Phys. 5, 2461–2474.

Szyszkowicz, M., Rowe, B., 2016. Respiratory health conditions and ambient ozone: a case-crossover study. Insights Chest Dis 1 (1) 9, 1-5.

Tarasick, D.W., Fioletov, V.E., Wardle, D.I., Kerr, J.B., Davies, J., 2005. Changes in the vertical distribution of ozone over Canada from ozonesondes: 1980-2001. J. Geophys. Res. 110, D02304. https://doi.org/10.1029/2004JD004643.

Tarasick, D.W., Jin, J.J., Fioletov, V.E., Liu, G., Thompson, A.M., Oltmans, S.J., Liu, J., Sioris, C.E., Liu, X., Cooper, O.R., Dann, T., Thouret, V., 2010. High-resolution tropospheric ozone fields for INTEX and ARCTAS from IONS ozonesondes. J. Geophys. Res. 115, D20301. https://doi.org/10.1029/2009JD012918.

Tarasick, D.W., Galbally, I.E., Cooper, O.R., Schultz, M.G., Ancellet, G., LeBlanc, T., Wallington, T.J., Ziemke, J., Liu, X., Steinbacher, M., Stähelin, J., Vigouroux, C., Hannigan, J., García, O., Foret, G., Zanis, P., Weatherhead, E., Petropavlovskikh, I., Worden, H., Neu, J.L., Osman, M., Liu, J., Lin, M., Granados-Muñoz, M., Thompson, A.M., Oltmans, S.J., Cuesta, J., Dufour, G., Thouret, V., Hassler, B., Thompson, A.M., Trickl, T., 2018. TOAR- Observations: How Well Do We Know Tropospheric Ozone Changes?, Manuscript in TOAR Open Comment, Prior to Submission to Elementa: Science of the Anthropocene.

Thompson, A.M., Stone, J.B., Witte, J.C., Pierce, R.B., Chatfield, R.B., J Oltmans, S., Cooper, O.R., Taubman, B.F., Johnson, B.J., Joseph, E., Kucsera, T.L., Merrill, J.T., Morris, G., Hersey, S., Newchurch, M.J., Schmidlin, F.J., Tarasick, D.W., Thouret, V., Cammas, J.-P., 2007a. Intercontinental chemical transport experiment ozonesonde network study (IONS) 2004: 1. Summertime upper troposphere/lower stratosphere ozone over northeastern north America. J. Geophys. Res. 112, D12S12. https://doi.org/10.1029/2006JD007441.

Thompson, A.M., Stone, J.B., Witte, J.C., Miller, S., J Oltmans, S., Kucsera, T.L., Merrill, J.T., Forbes, G., Tarasick, D.W., Joseph, E., Schmidlin, F.J., MacMillan, W.W., Warner, J., Hintsa, E., Johnson, J., 2007b. Intercontinental chemical transport experiment ozonesonde network study (IONS) 2004: 2. Tropospheric ozone budgets and variability over northeastern north America. J. Geophys. Res. 112, D12S13. https://doi.org/10.1029/2006JD007670.

Thompson, A.M., Oltmans, S.J., Tarasick, D.W., von der Gathen, P., Smit, H.G.J., Witte, J.C., 2010. Strategic ozone sounding networks: review of design and accomplishments. *Atmos. Environ.,* ISSN 1352–2310. https://doi.org/10.1016/j.atmosenv.2010.05.002.

Trickl, T., Feldmann, H., Kanter, H.-J., Scheel, H.-E., Sprenger, M., Stohl, A., Wernli, H., 2010. Forecasted deep stratospheric intrusions over Central Europe: case studies and climatologies. Atmos. Chem. Phys. 10, 499–524. https://doi.org/10.5194/acp-10-499-2010.

Trickl, T., Vogelmann, H., Giehl, H., Scheel, H.-E., Sprenger, M., Stohl, A., 2014. How stratospheric are deep stratospheric intrusions? Atmos. Chem. Phys. 14, 9941–9961. https://doi.org/10.5194/acp-14-9941-2014.

Trickl, T., Vogelmann, H., Fix, A., Schäfler, A., Wirth, M., Calpini, B., Levrat, G., Romanens, G., Apituley, A., Wilson, K.M., Begbie, R., Reichardt, J., Vömel, H., Sprenger, M., 2016. How stratospheric are deep stratospheric intrusions? LUAMI 2008. Atmos. Chem. Phys. 16, 8791–8815. https://doi.org/10.5194/acp-16-8791-2016.

Van Haver, P., De Muer, D., Beekmann, M., Mancier, C., 1996. Climatology of tropopause folds at midlatitudes. Geophys. Res. Lett. 23, 1033–1036. https://doi.org/10.1029/96GL00956.

Vanzandt, T.E., Green, J.L., Gage, K.S., Clark, W.L., 1978. Vertical profiles of refractivity turbulence structure constant: comparison of observations by the Sunset Radar with a new theoretical model. Rad. Sci. 13 (5), 819–829.

Vérèmes, H., Cammas, J.-P., Baray, J.-L., Keckhut, P., Barthe, C., Posny, F., Tulet, P., Dionisi, D., Bielli, S., 2016. Multiple subtropical stratospheric intrusions over Reunion Island: observational, Lagrangian, and Eulerian numerical modeling approaches. J. Geophys. Res. Atmos. 121 (14). https://doi.org/10.1002/2016JD025330. 414–14,432.

Wakamatsu, S., Uno, I., Ueda, H., Uehara, K., Tateishi, H., 1989. Observational study of stratospheric ozone intrusions into the lower troposphere. Atmos. Environ. 23, 1815–1826.

Wernli, H., Bourqui, M., 2002. A Lagrangian 1-year climatology of (deep) cross-tropopause exchange in the extratropical Northern Hemisphere. J. Geophys. Res. 107 (D2), 4021. https://doi.org/10.1029/2001JD000812.

WMO, 1966. International Meteorological Vocabulary. WMO, No. 182. TP. 91. Secretariat of the World Meteorological Organization, Geneva xvi, 276.

Zanis, P., Trickl, T., Stohl, A., Wernli, H., Cooper, O., Zerefos, C., Gaeggeler, H., Schnabel, C., Tobler, L., Kubik, P., Priller, A., Scheel, H.E., Kanter, H.J., Cristofanelli, P., Forster, C., James, P., Gerasopoulos, E., Delcloo, A., Papayannis, A., Claude, H., 2003. Forecast, observation and modelling of a deep stratospheric intrusion event over Europe. Atmos. Chem. Phys. 3, 763–777.

Zanis, P., Hadjinicolaou, P., Pozzer, A., Tyrlis, E., Dafka, S., Mihalopoulos, N., Lelieveld, J., 2014. Summertime free-tropospheric ozone pool over the eastern Mediterranean/Middle East. Atmos. Chem. Phys. 14, 115–132. https://doi.org/10.5194/acp-14-115-2014.